

# FUSION: Forecast-Embedded Agent Scheduling with Service Incentive Optimization over Distributed Air-Ground Edge Networks

Houyi Qi, Minghui Liwang, *Senior Member, IEEE*, Seyyedali Hosseinalipour, *Senior Member, IEEE*, Liqun Fu, *Senior Member, IEEE*, Sai Zou, *Senior Member, IEEE*, Xianbin Wang, *Fellow, IEEE*, Wei Ni, *Fellow, IEEE*, and Yiguang Hong, *Fellow, IEEE*

**Abstract**—We investigate a forecasting-driven, incentive-compatible service provisioning framework for distributed air-ground integrated edge networks under human-machine coexistence. We consider hybrid players where the computing capacity of edge servers (ESs) are augmented by vehicular-UAV agent pairs (AgPs) that can be proactively dispatched to overloaded hotspots. Unique key challenges should be addressed: highly uncertain spatio-temporal workloads, spatio-temporal coupling between road traffic and UAV capacity, forecast-driven contracting risks, and heterogeneous quality-of-service (QoS) requirements of human users (HuUs) and machine users (MaUs). To cope with these issues, we propose FUSION, a two-stage framework that tightly couples service demand prediction, agent deployment, and task scheduling. In the offline stage, a Pro-LNN module performs intelligent multi-step spatio-temporal demand forecasting at distributed ESs, whose outputs are exploited by an enhanced ant colony optimization-based routing scheme (eACOVRP) and an auction-based incentive-compatible contracting mechanism (Off-AIC<sup>2</sup>), to jointly determine ES-AgP contracts and pre-planned service routes. In the online stage, we formulate congestion-aware task scheduling as an potential game among HuUs, MaUs, and heterogeneous ES/UAV providers, and devise a potential-guided best-response dynamics (PG-BR) algorithm that provably converges to a pure-strategy Nash equilibrium. Extensive experiments on both synthetic and real-world traces show that FUSION significantly improves social welfare, latency, resource utilization, and robustness compared with state-of-the-art baselines.

**Index Terms**—Distributed edge computing, auction, liquid neural network, potential games, heterogeneous users.

## I. INTRODUCTION

WITH the rapid advancement of edge intelligence and unmanned aerial vehicle (UAV) technologies, a new generation of intelligent applications, such as real-time video analytics, intelligent transportation systems, and large-scale mobile crowdsensing, has flourished across smart cities [1], [2]. These applications are typically computation-intensive (e.g., calling for analyzing large amount of data, such as mode training and inference) and highly delay-sensitive, which imposes stringent requirements on the elasticity and quality

of edge services. Although edge servers (ESs) provide proximity computing capabilities, their geographically distributed deployment and limited local resources make them vulnerable to resource shortages and task congestion during peak periods, resulting in severe service latency and performance degradation [3].

To mitigate capacity limitations near the network edge, low-altitude-assisted edge computing has attracted extensive attention [4], [5]. Unlike static ESs, UAVs possess high flexibility and can be rapidly dispatched to hotspot regions to provide additional computing/caching capabilities. However, most existing studies implicitly assume that UAVs can “fly directly” to target regions, while overlooking practical constraints such as limited endurance and high deployment cost [6]–[9]. In large-scale urban scenarios with widely distributed ESs and hotspot regions (exhibit intricate spatio-temporal patterns), relying solely on UAV self-flight is insufficient to cover multiple overloaded ESs in time.

To this end, we advocate a *air-ground cooperative edge computing paradigm*: during periods of intensive demand, agents for service enhancement such as ground vehicles can be used to transport multiple UAVs (vehicles and UAVs are collectively known as “agent pairs (AgPs)” in our paper, each consisting of a vehicle as a carrier and several on-board UAVs) to the vicinities of overloaded ESs. UAVs are then launched from strategically selected locations to deliver temporary computational augmentation for nearby ESs [10], [11]. This not only expands on-demand computing capacity during peak intervals and alleviates ES congestion, but also enables more agile and fine-grained service provisioning for latency-sensitive applications. Despite these benefits, however, the introduction of UAV operations significantly increases system complexity across temporal, spatial, service, and economic dimensions. This complexity gives rise to several fundamental challenges that must be addressed to fully leverage the potential of this hybrid deployment paradigm.

**(A) High spatio-temporal demand uncertainty over complex environments with heterogeneous users.** Edge service demand exhibits pronounced spatio-temporal variability, and the coexistence of human users (HuUs) and machine users (MaUs)<sup>1</sup> further exacerbates the unpredictability of future workloads. This volatility makes it difficult to determine when, where, and

H. Qi (houyiqi@tongji.edu.cn), M. Liwang (minghuiliwang@tongji.edu.cn), and Y. Hong (yghong@iss.ac.cn) are with the Shanghai Research Institute for Intelligent Autonomous Systems, with the State Key Laboratory of Autonomous Intelligent Unmanned Systems, Frontiers Science Center for Intelligent Autonomous Systems, Ministry of Education, Shanghai Key Laboratory of Intelligent Autonomous Systems, and Department of Control Science and Engineering, Tongji University, Shanghai, China. S. Hosseinalipour (alipour@buffalo.edu) is with Department of Electrical Engineering, University at Buffalo–SUNY, NY, USA. L. Fu (liqun@xmu.edu.cn) is with School of Informatics, Xiamen University, Xiamen, China. S. Zou (dr-zousai@foxmail.com) is with College of Big Data and Information Engineering, Guizhou University, Guiyang, China. X. Wang (xianbin.wang@uwo.ca) is with the Department of Electrical and Computer Engineering, Western University, Ontario, Canada. W. Ni (Wei.Ni@ieee.org) is with Data61, CSIRO, Sydney, Australia.

Corresponding author: Minghui Liwang

<sup>1</sup>In this paper, we offer an unique perspective to distinguish between HuUs and MaUs: HuUs refer to individuals whose task performance directly affects their emotion or real-time experience (e.g., drivers using intelligent navigation, players engaged in mobile gaming and AR/VR). In contrast, MaUs denote non-human entities, such as mapping vehicles, delivery robots, or sensing units, whose task performance does not immediately or emotionally influence humans. Consequently, HuUs typically exhibit strict instantaneous latency sensitivity, while MaUs only require task completion within a pre-defined deadline window. These differences lead to fundamentally heterogeneous QoS requirements, and thus utility modelings in subsequent sections.

how UAV resources should be dispatched. Static provisioning or purely reactive scheduling often leads to mismatches between supply and demand, manifesting as severe congestion in emerging hotspots and resource underutilization in low-demand regions [12], [13]. The core challenge, therefore, lies in developing accurate and actionable multi-step spatio-temporal demand forecasts based on historical requests and contextual information. Such forecasts are essential for enabling proactive, rather than reactive, UAV deployment decisions; yet achieving reliable predictions under highly dynamic and heterogeneous urban environments remains fundamentally difficult.

**(B) Spatio-temporal coupling in complexity of road traffic networks and capacity of UAVs.** During peak periods, AgPs can serve overloaded ESs that are geographically distributed. However, vehicular mobility is constrained by road network topology, traffic dynamics, and strict time budgets, while the number of UAVs that each vehicle can deploy is tightly coupled with its visiting sequence and dwell duration at each ES. These spatio-temporal dependencies create a highly entangled decision space. As a result, the underlying vehicle-UAV joint deployment optimization becomes strongly NP-hard, where plans must simultaneously incorporate multi-modal travel costs, strict service time windows, UAV dispatching logistics, and the spatially distributed service rewards linked to relieving ES overload. This tight coupling yields a highly interdependent decision space.

**(C) Predictive contracting and incentive-compatible trading.** To facilitate timely services, ESs can buy services from AgPs, calling for establishing advance contracts, committing to service capacity and pricing for future peak intervals before those intervals materialize. However, inevitable forecasting errors and dynamically evolving supply-demand conditions introduce substantial risks for both parties: ESs may face unmet demand if the contracted capacity falls short, whereas AgPs may incur stranded capacity or loss from misallocated resources. The central challenge lies in designing an offline trading mechanism that remains individually rational, incentive compatible, and budget feasible [14], while explicitly integrating predictive uncertainty into the contracting process. Achieving such robustness without sacrificing economic efficiency or strategic truthfulness is nontrivial, making it a fundamental difficulty in forecast-driven agents collaboration.

**(D) Timely and fairness-aware online coordination under heterogeneous human-machine coexistence.** When actual computing demands arrive, HuUs and MaUs may compete for the same pool of resources provided by local ESs and leased UAVs. However, their quality-of-service (QoS) requirements differ fundamentally: HuUs are highly sensitive to instantaneous delay (their emotion can directly be affected), whereas MaUs primarily value timely task completion before deadlines. In proper coordination can lead to individually rational behaviors and unsatisfying services, such as inequitable resource distribution across heterogeneous user groups, recurrent congestion oscillations among ESs, and sub-optimal utilization of UAV-enhanced service capacity. The key challenge is thus to design fairness-aware distributed scheduling with provable convergence guarantees, ensuring both equitable treatment across heterogeneous user types and high system-wide efficiency in human-machine coexistence environments.

These above challenges collectively underscore the core motivation of our work. In this paper, we develop a forecasting-driven agent scheduling (i.e., AgPs formed by vehicles and

UAVs) and incentive optimization (FUSION) framework for edge service provision, with two stages involved: seamlessly integrating demand prediction, agent and task scheduling, and incentive design. First, for challenge (A), we design a proactive spatio-temporal demand prediction via liquid neural networks (*Pro-LNN*), transforms historical service traces and contextual features into multi-step workload forecasts, thereby offering actionable decision support for effective AgP deployment. Then, for challenge (B), we propose an enhanced ant colony optimization for vehicular rout planning (*eACO-VRP*) based on the predicted demand, jointly models ESs' demand time windows, vehicular travel cost, and expected deployment rewards, generating cost-effective and executable plans. Third, for challenge (C), we introduce offline auction-based incentive-compatible contracting (*Off-AIC<sup>2</sup>*) that matches ESs with proper AgPs, determines payments and rewards, thereby achieving, to a certain extent, individual rationality, incentive compatibility, and budget feasibility. Finally, for challenge (D), we formulate an efficient online potential game among HuUs, MaUs, and heterogeneous ES/UAV, and propose the potential game-based best-response dynamics (*PG-BRD*) method, which integrates potential-guided dual decomposition with asynchronous best-response dynamics to drive the system towards a pure-strategy Nash equilibrium (NE) under congestion and fairness constraints. To sum up, our principal contributions are summarized as follows:

- We investigate a distributed air-ground integrated edge network architecture that holistically models the deep coupling among AgPs, and ESs, together with the heterogeneous computing demands arising in human-machine coexistence. To enable seamless, intelligent, and latency-sensitive service delivery, we cast the goal as a unified optimization with NP-hardness, due to intertwined mobility patterns, stochastic workloads, and strategic agent behaviors. To cope with this, we offer an unique view, spanning spatio-temporary demand prediction, agent scheduling, and incentive-compatible coordination, by designing two complementary stages.
- We first construct a prediction-driven offline optimization stage, where *Pro-LNN* is designed to perform multi-step spatio-temporal workload prediction by training LNNs; while *eACO-VRP* exploits the prediction to jointly consider ES time windows, travel cost, and expected rewards, producing cost-effective and practically executable vehicular routings as well as UAV pre-deployment plans. Besides, during this stage, we investigate *Off-AIC<sup>2</sup>* that conducts auction-based matching and pricing between ESs and AgPs under predicted supply-demand conditions. Also, to ensure the effectiveness with explainability of our methodology, we offer theoretical analysis on individual rationality, incentive compatibility, and budget feasibility proofs under mild conditions.
- Then, we turn to an online stage, wherein the scheduling process is modeled as a potential game among HuUs, MaUs, and heterogeneous ES/UAV, and develop a method called *PG-BR*, with convergence proof to a pure-strategy NE over controlled congestion and guaranteed fairness.
- Extensive experiments based on real-world datasets demonstrate that our *FUSION* significantly reduces latency, improves resource utilization, and enhances robustness compared with state-of-the-art benchmarks.

## II. LITERATURE REVIEW

### A. Service Provision in UAV-Assisted Edge Networks

UAV-assisted edge computing [6]–[9] extends computation beyond static infrastructures, with resource scheduling coordinating communication, computation, and mobility. Existing studies primarily focus on efficiency, communication performance, and energy reduction in UAV-ground interactions. For instance, *Wang et al.* [6] designed a multi-agent deep reinforcement learning (MADRL)-based distributed scheduling scheme for intelligent reflecting surface (IRS)- and UAV-assisted wireless powered edge networks. *Xu et al.* [7] studied UAV-assisted internet of things (IoT) inference via DRL with an embedded resource allocation subroutine to minimize average inference delay. *Li et al.* [8] investigated federated edge intelligence for UAV-enabled IoT networks to jointly minimize UAV uploading energy and improve edge resource utilization. *Zeng et al.* [9] developed edge-server-assisted drone navigation via a DRL-based neural scheduler and network-aware containerized resource allocation to maximize a quality-of-navigation metric.

Although the above studies offer valuable insights, they predominantly rely on static or quasi-static geometric models that implicitly assume the UAV is always “nearby” and can provide immediate service. Consequently, they overlook critical factors such as UAV flight time, positional evolution, task arrival time, and the dynamic accessibility of ESs. Nevertheless, in practical arrival time, service sequencing, trajectory-dependent accessibility, and spatio-temporally varying workloads of UAVs play essential roles. These characteristics call for a transition from static coverage-based optimization toward spatio-temporal-aware frameworks.

### B. Auction-Driven Service Delivery over Distributed Edge Networks.

Auctions have been extensively investigated as an incentive-compatible paradigm over edge networks, enabling strategic users and heterogeneous service providers to transact multi-type services. For instance, *Ren et al.* [15] investigated truthful auctions for dependent task scheduling to maximize system utility in dynamic environments. *Xu et al.* [16] designed combinatorial auction-based distributed deep neural network (DNN) inference for heterogeneous edge–cloud networks to maximize social welfare. *Li et al.* [17] developed an online auction for artificial intelligence generated content (AIGC) task scheduling to optimize decisions on instances and time schedules. *Lu et al.* [18] presented auction-based cluster federated learning to improve convergence and balance energy consumption in edge networks.

While the above studies provide insights into incentive-compatible service provision in edge systems, they are mostly single-stage, reactive, and assume fixed resources and stable demand. This leads to high signaling overhead, latency, and energy costs, especially for large numbers of battery-constrained devices. In UAV-assisted edge computing, dynamic resources, bursty task arrivals, and strict delay/energy constraints call for time-efficient, spatio-temporal aware auction frameworks that reduce online interactions while handling real-world uncertainties.

TABLE I

A SUMMARY OF RELATED STUDIES  
(ST: SPATIO-TEMPORAL, PRED.: PREDICTIVE, HET.: HETEROGENEOUS)

Reference	Network Characteristics			Service Delivery			Participant	
	Static	Dynamic	ST	Offline	Online	Pred.	Het. users	Het. ESs
[6]		√	√		√			
[7]		√			√		√	
[8]		√		√				√
[9]		√			√			
[12], [19], [20]	√			√				√
[13]	√			√				√
[15]		√	√	√			√	√
[16], [17]		√			√		√	√
[18]		√		√			√	
<b>Our Work</b>		√	√	√	√	√	√	√

### C. Game-empowered Service Provision over Distributed Edge Networks

Beyond auctions, potential-game-based approaches also explored distributed optimization strategies for edge service provisioning [12], [13]. *Ding et al.* [12] investigated end–edge–cloud computing architectures, formulating task assignment among different parties as potential games. *Zhou et al.* [13] modeled a potential game with latency–energy trade-off utilities to a pure-strategy NE. *Hsieh et al.* [19] proposed a knapsack potential game for task scheduling, aiming to balance QoS guarantees for different traffic priorities and overall cost-effectiveness. *Wu et al.* [20] developed a potential-game-based task scheduling scheme for multi-cell edge–cloud collaboration to a NE while minimizing users’ joint delay–energy cost.

Overall, potential-game-based studies show that carefully designed utilities and potential functions can achieve convergent, distributed scheduling equilibrium and reduce system costs. However, they generally consider a single, homogeneous user type, ignoring the distinct delay sensitivities and utility structures of HuUs and MaUs, as well as their interactions with heterogeneous ESs. Consequently, UAV-assisted platforms supporting human-machine coexistence, spatio-temporal task windows, and multi-party potential games remain largely unexplored. To highlight our contributions, Table I compares our work with representative existing studies.

## III. OVERVIEW AND MODELING

### A. Overview of Our Methodology

We consider an air–ground integrated edge network, where all participants can be naturally grouped into two key categories: *service demanders* and *service providers*.

1) *Service demanders (SDs)*. This includes users that generate tasks such as model training/inference<sup>2</sup>. To capture fundamentally different QoS needs over human-machine coexistence, we further classify them into two groups:

- **HuUs**, denoted by  $\mathcal{U}^H = \{u_1^H, \dots, u_{|\mathcal{U}^H|}^H\}$ . HuUs are strongly sensitive to instantaneous service latency, as applications such as AR/VR, interactive gaming, real-time video conferencing, and intelligent driving can directly influence their experience and further emotion. Even slight increases in latency or service degradation may leave a heavy impact on their perceived utility.

<sup>2</sup>We assume that each SD is associated with one task that requires computing services from SPs in every future trading round.

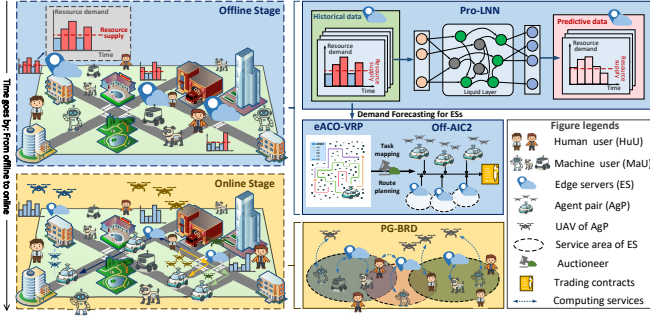


Fig. 1. Schematic of our FUSION over distributed air-ground integrated edge network.

- **MaUs**, denoted by  $\mathcal{U}^A = \{u_1^A, \dots, u_{|\mathcal{U}^A|}^A\}$ . MaUs correspond to autonomous devices such as robots, mapping vehicles, and sensing units. They primarily care about whether missions can be completed before a certain deadline, and are therefore less impacted by instantaneous latency, as long as overall task feasibility is preserved.

The coexistence of motion-sensitive HuUs and mission-oriented MaUs brings heterogeneous utility structures, imposing substantial challenges for optimized service delivery.

2) *Service providers (SPs)*. This consists of two types of computing infrastructures:

- **ESs**, denoted by  $\mathcal{S} = \{s_1, \dots, s_{|\mathcal{S}|}\}$ , which are geographically distributed across the map and provide low-latency services to nearby users. Each ES operates with a limited pool of orthogonal subcarriers and finite capacity, inherently constraining the number of users that can be concurrently served. During peak-demand periods, hotspot ESs are particularly susceptible to resource saturation, which can trigger substantial queuing delays or even outright admission blocking.
- **AgPs**, denoted by  $\mathcal{V} = \{v_1, \dots, v_{|\mathcal{V}|}\}$ , with each formed by a vehicle with multiple UAVs charging on-board. Due to the limited power of UAVs, vehicles are firstly hired to traverse pre-planned routes, act as mobile carriers that transport UAVs to designated service locations. Upon approaching their contracted ESs, UAVs are deployed to offer local computing enhancing assistance. However, this paradigm also incurs non-trivial operational costs, including vehicle repositioning, UAV dispatch and launch procedures, flight energy consumption, and maintenance overhead.

Under this two-sided demand-supply structure, SDs compete for low-latency, reliable computing services, while SPs collaboratively offer computing resources under capacity and operational limitations. Nevertheless, in such a dynamic ecosystem, each ES can face *uncertain service demand*: the temporal and spatial distribution of service request peaks at each ES is highly stochastic, and the composition ratio between HuUs and MaUs in the service requests also varies dynamically over time.

Against this background, we develop hybrid and coupled stages. As illustrated in Fig. 1, the offline stage first trains an LNN to perform multi-step spatio-temporal forecasting of future service demand at each ES. Guided by this, we jointly plan vehicular visiting routes and the initial deployment of UAVs, while simultaneously designing auction-driven incentive for trading contracts between ESs and AgPs. In *online Stage*, interactions among SDs (e.g., HuUs and MaUs), and heterogeneous SPs (e.g., ESs and UAVs) are modeled by forming a

potential game. By constructing an ordinal potential function to capture the global utility, we allow each player updates its strategy locally and the overall performance converges to a pure-strategy NE, yielding a near-global optimal solution.

In summary, our ultimate goal is to *design a sustainable, intelligent, and incentive-compatible framework for distributed edge service provision, that organically integrates forecasting-driven offline contracting with game-based online scheduling, so as to balance service performance and operational cost, further achieving multi-party win-win over human-machine coexistence.*

## B. Basic Modeling

In the following, we offer detailed modelings for players.

1) *Modeling of SDs*: Recall previous discussions, we model HuUs and MaUs respectively.

(i) **For HuUs**: Each HuU  $u_m^H \in \mathcal{U}^H$  is modeled by a 5-tuple  $u_m^H = \{e_m^{H,tx}, r_m^H, d_m^H, f_m^{H,loc}, C_m^H\}$ , where  $e_m^{H,tx}$  is the uplink transmit power (Watts);  $r_m^H$  is the required computing workload (CPU cycles);  $d_m^H$  is the input data size (bits);  $f_m^{H,loc}$  is the local CPU frequency; and  $C_m^H$  represents the set of reachable ESs within the communication coverage of  $u_m^H$ .

(ii) **For MaUs**: Each MaU  $u_n^A \in \mathcal{U}^A$  is represented by a 6-tuple  $u_n^A = \{\tau_n^{ddl}, e_n^{A,tx}, r_n^A, d_n^A, f_n^{A,loc}, C_n^A\}$ , where  $\tau_n^{ddl}$  is the task deadline time;  $e_n^{A,tx}$  is the transmit power;  $r_n^A$  and  $d_n^A$  denote the required workload and data size, respectively.  $f_n^{A,loc}$  is its local CPU capability, and  $C_n^A$  is the set of SPs that can serve  $u_n^A$ .

Note that one unique aspect appears in our paper: HuUs exhibit strong latency sensitivity, e.g., even minor delays can noticeably degrade their experience and affect their emotions. In contrast, MaUs are predominantly goal-driven and primarily require that their tasks be completed before predefined deadlines. This fundamental distinction results in heterogeneous scheduling priorities and markedly different utility structures.

2) *Modeling of SPs*: Regarding two types of SPs, we have detailed models below.

(i) **For ESs**: Each ES  $s_i \in \mathcal{S}$  is characterized by a 4-tuple:  $s_i = \{f_i^E, e_i^E, G_i, l_i^E\}$ , where  $f_i^E$  is the computing capacity (e.g., CPU cycles/s);  $e_i^E$  is its local power consumption (Watts); In addition, each ES  $s_i$  has a set of orthogonal subcarriers that can serve at most  $G_i$  SDs simultaneously; and  $l_i^E = (x_i^E, y_i^E, h_i^E)$  denotes its fixed 3D location.

(ii) **For AgPs**: each AgP  $v_k \in \mathcal{V}$  is modeled by a 7-tuple:  $v_k = \{C_k^V, f_k^V, e_k^{comp}, e_k^{move}, e_k^{fly}, G_k^V, l_k^V\}$ , where  $C_k^V$  denotes the maximum number of UAVs carried by the vehicle;  $f_k^V$ : computing capability of each mounted UAV;  $e_k^{move}$ ,  $e_k^{comp}$ , and  $e_k^{fly}$  refer to power consumed for ground movement, UAV computation, and UAV flight, respectively;  $G_k^V$  denotes the maximum number of SDs that each UAV of  $v_k$  can serve, owing to the use of orthogonal subcarriers, and  $l_k^V = (x_k^V, y_k^V, H_0^V)$  is the ground location of the dispatching vehicle.

**Modeling of offline contracts**: In the offline stage, a trading contract is established between each ES  $s_i$  and AgP  $v_k$ , denoted as  $\mathbb{C}_{i,k}^{E \leftrightarrow V} = \{N_{i,k}^{Trad}, p_i^{ES}, r_{i,k}^{ES}\}$ , where  $N_{i,k}^{Trad}$  represents the quantity of traded resources,  $p_i^{ES}$  indicates unit payment (per task) from  $s_i$  to contractual AgP  $v_k$ , and  $r_{i,k}^{ES}$  refers to the unit reward (per task) of  $v_k$  for offering services.

#### IV. OFFLINE STAGE: FORECASTING-DRIVEN CONTRACTING AND AGP DEPLOYMENT

This section systematically transforms uncertain spatio-temporal service demand into proactive, incentive-compatible, and cost-aware agent deployment decisions. Our major efforts include: (i) a predictive workload forecasting module that estimates the spatiotemporal dynamics of demands across distributed ESs; (ii) a cost-aware vehicle routing strategy based on eACO, which constructs time-window-feasible candidate associations between AgPs and ESs; and (iii) a contract-design module that leverages an incentive-compatible auction mechanism to determine long-term cooperative agreements, including winning trading pairs, allocated resources, and corresponding payment rules.

To facilitate analysis, let  $x_{i,k}^{\text{Off}}$  denote the assignment between ESs and AgPs, where  $x_{i,k}^{\text{Off}} = 1$  indicates that ES  $s_i$  successfully secures the service of AgP  $v_k$  and thereby signs an offline contract, and  $x_{i,k}^{\text{Off}} = 0$  otherwise. For notational simplicity, we define  $\mathbf{X}^{\text{Off}} = \{x_{i,k}^{\text{Off}} \mid s_i \in \mathcal{S}, v_k \in \mathcal{V}\}$  as the assignment profile.

##### A. Utility of ESs, AgP, and Auctioneer

1) *Utility of ESs*: In the offline stage, since delivering edge services to users and leasing computing capacity can generate both costs and revenues for ESs, we model the utility of each ES  $s_i$  as its net profit<sup>3</sup>, i.e., revenue from serving users minus payments for buying services from AgP  $v_k$ . Formally, the profit of ES  $s_i$  is given by

$$U_i^{\text{ES,Off}} = \sum_{v_k \in \mathcal{V}} x_{i,k}^{\text{Off}} N_{i,k}^{\text{Trad}} (\bar{p}_i - p_{i,k}^{\text{ES}}) \quad (1)$$

where  $\bar{p}_i$  denotes the historical average payment earned by  $s_i$  for providing edge services to users.

2) *Utility of AgPs*: For each AgP, we model its utility in terms of four key components: (i) *Vehicular moving cost*: the energy cost incurred by the vehicle traveling to ES  $s_i$  is  $c_{i,k}^{\text{move}} = \tau_{i,k}^{\text{move}} e_k^{\text{move}}$ , where  $\tau_{i,k}^{\text{move}}$  denote the traveling time of the carrier vehicle when moving from its origin to the target ES  $s_i$ , which depends on the driving distance and the AgP's vehicular speed; (ii) *UAV flying cost*: the energy consumption during UAV flight is  $c_{i,k}^{\text{fly}} = \tau_{i,k}^{\text{fly}} e_k^{\text{fly}}$ , where  $\tau_{i,k}^{\text{fly}}$  denote the total UAV flight time spent shuttling between  $s_i$  and its associated service region, which increases with the number and size of the tasks to be served; (iii) *UAV computing cost*: the energy consumed by UAV while assisting edge services is  $c_{i,k}^{\text{comp}} = \tau_{i,k}^{\text{comp}} e_k^{\text{comp}} = \frac{\bar{r} e_i^{\text{E}}}{f_k^{\text{V}}}$ , where  $\bar{r}$  denotes the historical average computational workload per task<sup>4</sup>, and  $\tau_{i,k}^{\text{comp}}$  represent the effective computing time that the UAV dedicates to processing offloaded tasks, determined by the aggregate computational workload and the UAV's computing capability; and (iv) *Income for service provisioning*: the revenue obtained from contributing edge services is denoted by  $r_{i,k}^{\text{ES}}$ . The overall utility of  $v_k$  can therefore be expressed as

$$U_k^{\text{V}} = \sum_{s_i \in \mathcal{S}} x_{i,k}^{\text{Off}} \omega_1 (r_{i,k}^{\text{ES}} - c_{i,k}^{\text{move}} - c_{i,k}^{\text{fly}} - N_{i,k}^{\text{Trad}} c_{i,k}^{\text{comp}}) + \omega_2 c^{\text{hard}}, \quad (2)$$

<sup>3</sup>In the online stage considered here, SDs can offload tasks directly to UAVs for execution; therefore, the ES's utility does not account for any energy cost of transmitting tasks from the ES to UAVs.

<sup>4</sup>Since trading is conducted in the offline stage, AgPs do not know the exact sizes of the tasks they will eventually process and can only evaluate them based on historical average data.

where  $\omega_1$  and  $\omega_2$  denote cost coefficients that convert energy consumption into monetary units (e.g., dollars), and  $c^{\text{hard}}$  represents the hardware depreciation cost.

3) *Utility of the Auctioneer*: Since trading contracts are driven by a well-designed auction process, we involve an auctioneer (e.g., acted by a trusted third party), playing a pivotal role in coordinating interactions among players, including bids/asks collection, winning AgPs-ESs determination, and trading contract design. Accordingly, utility of the auctioneer generally depends on the difference between the total income obtained by AgPs and the expense paid by ESs:

$$U^{\text{Auc}} = \sum_{s_i \in \mathcal{S}} \sum_{v_k \in \mathcal{V}} x_{i,k}^{\text{Off}} N_{i,k}^{\text{Trad}} (p_{i,k}^{\text{ES}} - r_{i,k}^{\text{ES}}), \quad (3)$$

##### B. Problem of Our Interest in Offline Stage

A fundamental and critical goal within an auction market is to maximize its social welfare (SW), for which we design as the collective utilities of three parties (e.g., ESs, AgPs, auctioneer), as given by:

$$U^{\text{SW}} = \sum_{s_i \in \mathcal{S}} U_i^{\text{ES,Off}} + \sum_{v_k \in \mathcal{V}} U_k^{\text{V}} + U^{\text{Auc}}. \quad (4)$$

During this offline stage, our primary objective is to determine the optimal winning ES-AgP pairs (requiring obtaining  $x_{i,k}^{\text{Off}}$  combinations), while establishing their corresponding trading contracts, e.g.,  $\mathbb{C}_{i,k}^{\text{E} \leftrightarrow \text{V}}$ . This is formulated by an optimization problem  $\mathcal{F}^{\text{I}}$ , as expressed in (5).

$$\mathcal{F}^{\text{I}}: \underset{x_{i,k}^{\text{Off}}, \mathbb{C}_{i,k}^{\text{E} \leftrightarrow \text{V}}}{\text{argmax}} U^{\text{SW}} \quad (5)$$

$$\text{s.t.} \quad \sum_{v_k \in \mathcal{V}} x_{i,k}^{\text{Off}} \leq 1, \quad \forall s_i \in \mathcal{S} \quad (5a)$$

$$x_{i,k}^{\text{Off}} \in \{0, 1\}, \quad \forall s_i \in \mathcal{S}, \forall v_k \in \mathcal{V} \quad (5b)$$

$$\sum_{s_i \in \mathcal{S}} x_{i,k}^{\text{Off}} N_{i,k}^{\text{Trad}} \leq G_k^{\text{V}}, \quad \forall v_k \in \mathcal{V} \quad (5c)$$

where constraint (5a) ensures that each ES is matched with a unique AgP, and (5b) enforces the binary nature of  $x_{i,k}^{\text{Off}}$ . Constraint (5c) guarantees that the promised resources in signed contracts do not exceed the actual supply provided by  $v_k$ .

Apparently,  $\mathcal{F}^{\text{I}}$  can be cast as a mixed-integer linear programming (MILP) problem that involves both discrete variables (e.g.,  $x_{i,k}^{\text{Off}}$ ) and continuous variables (e.g.,  $\mathbb{C}_{i,k}^{\text{E} \leftrightarrow \text{V}}$ ), and is therefore NP-hard [21], [22]. Rather than solving this directly, we observe that the quality of any auction-based solution fundamentally depends on how accurately the future resource usage can be predicted. Motivated by this, in the following, we first develop Pro-LNN to capture the spatio-temporal demands of ESs; then, based on these forecasts, we design eACO-VRP to plan AgPs' service routes and recommend suitable ES sets. Building on these two components, we further design an Off-AIC<sup>2</sup> that determines the winning ES-AgP pairs together with their contracts.

##### C. Forecasting, Agent Deployment and Contracting

To address the complex problem  $\mathcal{F}^{\text{I}}$ , we develop LNN-empowered proactive forecasting for future demands, vehicular routing (using eACO), as well as auction-driven contracting.

1) *Design of Proactive Spatio-Temporal Demand Prediction via Liquid Neural Networks (Pro-LNN)*: Unlike discrete-time RNNs or Transformers, LNNs [23] rely on exponential-style state updates with neuron-wise time constants, making them naturally suited for irregular sampling, non-stationary patterns, and lightweight edge deployment. In our setting, the service demand of each ES exhibits strong spatio-temporal variability with occasional missing or uneven observations. Hence, the predictor must remain stable under irregular effective time gaps (denoted by  $\Delta v$ ) while capturing both short-lived bursts and long-term trends, where  $\Delta v$  represents the time interval between two consecutive trading rounds. To avoid confusion with the fine-grained time-slot index used in the online stage, we use the Greek letter  $v$  to index trading rounds throughout this subsection.

Let  $N_i^{\text{Dem},(v)}$  denote the task demand of ES  $s_i$  at the  $v$ -th trading round, and  $\mathbf{z}_i^{(v)} = [N_i^{\text{Dem},(v)}, \mathbf{x}_i^{(v)}]$  collect the demand and optional exogenous features. Given a length- $L$  history  $\{\mathbf{z}_i^{(v-L+1)}, \dots, \mathbf{z}_i^{(v)}\}$ , Pro-LNN encodes this sequence via a stable liquid cell with neuron-wise time constants, integrates the observations into a hidden state  $\mathbf{h}_i^{(v)}$ , and then applies a shallow readout network to produce an  $H$ -step forecast  $\{\hat{N}_i^{\text{Dem},(v+1)}, \dots, \hat{N}_i^{\text{Dem},(v+H)}\}$ . The model is trained with an  $H$ -step MSE loss, optionally augmented by a multi-step consistency term that rolls the predictor forward in closed loop and penalizes accumulated errors at future trading rounds. These forecasts are computed offline before each trading round and then fed into the eACO-VRP module for ES recommendation and AgP route pre-planning, as well as the auction module for ES-AgP contract design. The detailed update equations and training pseudocode of Pro-LNN are deferred to Appx. B (Algorithm 4) due to space limitations.

2) *Enhanced Ant Colony Optimization for Vehicle Route Planning (eACO-VRP)*: Inspired by ACO [25], [26] and tailored to the heterogeneity of ESs (e.g., distinct time windows and locations) and AgPs (e.g., diverse costs), we develop a method called eACO-VRP (Alg. 1). The scheme encourages each AgP to select a set of ESs and a pre-planned service route (i.e., an ES visiting sequence) to be served, to maximize its utility. For a given  $v_k$ , we model  $v_k$  and all ESs as vertices of a directed complete graph  $\mathcal{G}_k(\mathcal{N}_k, \mathcal{E}_k)$ . Here,  $\mathcal{N}_k = \{n_0, n_1, \dots, n_{|S|}\}$  denotes vertex set, where  $n_0$  represents  $v_k$  and  $n_1, \dots, n_{|S|}$  denote ESs; while the edge set is  $\mathcal{E}_k = \{(n_r, n_s) \mid n_r, n_s \in \mathcal{N}_k, r \neq s\}$ . Let the location of  $n_0$  be  $\ell_k^v(0)$ , and the locations of  $n_1, \dots, n_{|S|}$  be  $\ell_1^s, \dots, \ell_{|S|}^s$ , respectively.

We denote  $\mathbb{K}$  as the set of ants. Each ant  $k \in \mathbb{K}$  simulates the trajectory of  $v_k$ , starting from  $n_0$ . At each step, it evaluates: the current timeslot, ES time windows, vertex locations, the travel time to each candidate ES, and the utility upon arrival; it then selects a feasible next vertex to visit (i.e., whether the arrival time from the current vertex plus travel time remains before the end of the candidate vertex's time window). This process continues until no visitable vertex remains. The state-transition rule, i.e., the probability that ant  $k$  moves from

---

### Algorithm 1: Proposed eACO-VRP

---

```

1 Input: AgP  $v_k$  (source node  $n_0$ ), ES set  $\mathcal{S}$ , directed complete graph
    $\mathcal{G}_k(\mathcal{N}_k, \mathcal{E}_k)$ , ant set  $\mathbb{K}$ , max iterations  $iter_{\max}$ 
2 Initialization:  $\varphi_{r,s} \leftarrow \varphi_0$  for all  $(n_r, n_s) \in \mathcal{E}_k$ ;  $iter \leftarrow 1$ 
3 while  $iter \leq iter_{\max}$  do
4   for each ant  $k \in \mathbb{K}$  do
5      $M^k \leftarrow \emptyset$ ;  $n_{\text{cur}} \leftarrow n_0$ 
6     while end condition not met do
7       Compute: feasible set  $J_k(n_{\text{cur}})$  and transition
          probabilities  $p_{n_{\text{cur}} \rightarrow n_s}^k$  (via (6))
8       if  $J_k(n_{\text{cur}}) \neq \emptyset$  then
9         sample next node  $n_{\text{next}} \sim p_{n_{\text{cur}} \rightarrow n_s}^k$  over
           $n_s \in J_k(n_{\text{cur}})$ 
10         $M^k \leftarrow M^k \cup \{\text{edge}(n_{\text{cur}}, n_{\text{next}})\}$ 
11         $n_{\text{cur}} \leftarrow n_{\text{next}}$ 
12      else
13        break
14     $M^{\max} \leftarrow \arg \max_{M^k: k \in \mathbb{K}} \sum_{(n_r, n_s) \in M^k} \overline{\Delta U_{r,s}^W}$ 
15    for each  $(n_r, n_s) \in \mathcal{E}_k$  do
16      Pheromone evaporation and deposit (7) and (8)
17     $iter \leftarrow iter + 1$ 
18 Output:  $M^{\max}$  (pre-planned route for  $v_k$ ), and the recommended ES
          tasks along  $M^{\max}$ 

```

---

$n_r$  to  $n_s$  ( $r \neq s \neq 0$ ), is given by (6), with positive weights  $\varepsilon_1, \varepsilon_2, \varepsilon_3, \varepsilon_4$ . We denote by  $\varphi_{r,s}$  the pheromone level on edge  $(n_r, n_s)$  (see (7));  $\eta_{r,s}$  is the distance between  $n_r$  and  $n_s$ ; the time-window width at vertex  $n_s$  is  $\text{width}_s = t_s^e - t_s^b$ . If the ant arrives early (e.g., before the ES demand window starts), the waiting time  $\text{wait}_s$  is defined as the arrival time minus the starting time of the ES's demand window. Let  $J_k(r)$  be the set of feasible ES vertices that ant  $k$  can still complete when standing at node  $n_r$ . An ES  $n_s \in J_k(r)$  must satisfy two feasibility conditions: (i) the current time plus the travel time from  $n_r$  to  $n_s$  does not exceed the starting time of  $s$ 's demand window, and (ii) the current UAV load of AgP  $v_k$  is sufficient to satisfy the demand of  $n_s$ .

Once a route is found by the colony, pheromones on edges are updated by

$$\varphi_{r,s} \leftarrow (1 - \theta) \varphi_{r,s} + \Delta \varphi_{r,s}, \quad (7)$$

where  $0 < \theta < 1$  is the evaporation coefficient, and the deposited pheromone is

$$\Delta \varphi_{r,s} = \begin{cases} \sum_{(n_r, n_s) \in M^{\max}} \Delta U_{r,s}^V, & \text{if } (n_r, n_s) \in M^{\max}, \\ 0, & \text{otherwise,} \end{cases} \quad (8)$$

where  $\Delta U_{r,s}^V$  denotes the utility increment for  $v_k$  when moving from  $n_r$  to serve the ES at  $n_s$ . The path with the largest utility among all ants is  $M^{\max} = \{M^k \mid \max \sum_{(r,s) \in M^k} \Delta U_{r,s}^V, \forall k \in \mathbb{K}\}$ . Alg. 1 details the pseudo-code of eACO-VRP:

**Step 1. Initialization.** Using the AgP/ES profile information

$$p_{n_r \rightarrow n_s}^k = \begin{cases} \frac{\varphi_{r,s}^{\varepsilon_1} \eta_{r,s}^{\varepsilon_2} (1/\text{width}_s)^{\varepsilon_3} (1/\text{wait}_s)^{\varepsilon_4}}{\sum_{n_q \in J_k(n_r)} \varphi_{r,q}^{\varepsilon_1} \eta_{r,q}^{\varepsilon_2} (1/\text{width}_q)^{\varepsilon_3} (1/\text{wait}_q)^{\varepsilon_4}}, & \text{if } n_s \in J_k(n_r), \\ 0, & \text{otherwise.} \end{cases} \quad (6)$$

(e.g., geographic locations, ES time windows, AgP  $v_k$  obtains payments and service costs, and the travel/service time and energy), we construct, for each AgP  $v_k$  (with source node  $n_0$ ), a directed complete graph  $\mathcal{G}_k(\mathcal{N}_k, \mathcal{E}_k)$ . The node set  $\mathcal{N}_k$  contains the depot and all candidate ES vertices, while the edge set  $\mathcal{E}_k$  encodes pairwise connectivity together with the associated travel and service attributes that will be used during route construction.

**Step 2. Path exploration.** At each iteration, an ant  $\mathbb{k}$  located at its current vertex  $n_r$  jointly evaluates the current time, the travel time to each unvisited vertex, the service time at that vertex, and the corresponding time-window constraint to determine feasibility. This screening step yields the feasible candidate set  $J_{\mathbb{k}}(r)$  and the associated transition probabilities  $pr_{r,s}^{\mathbb{k}}$  (line 7, Alg. 1). The ant then stochastically selects its next vertex from  $J_{\mathbb{k}}(r)$  according to (6). The construction of a path for ant  $\mathbb{k}$  terminates once no executable vertex remains (line 13, Alg. 1).

**Step 3. Pheromone update.** For each constructed path  $M^{\mathbb{k}}$ , we compute the cumulative utility  $\sum_{(r,s) \in M^{\mathbb{k}}} \Delta U_{r,s}^{\mathbb{k}}$ . Among all ants, the path with the largest utility is selected as  $M^{\max}$ , and the pheromone trails on its edges are reinforced (lines 14-16, Alg. 1) according to the update rules in (7) and (8), while pheromones on other edges evaporate.

**Step 4. Output.** After all iterations, the route  $M^{\max}$  with the highest utility is returned as the pre-planned path for AgP  $v_k$ , and the ES tasks located along this route are recommended as its preferred service targets.

3) *Offline Auction-based Incentive-Compatible Contracting (Off-AIC<sup>2</sup>):* Following the pre-planned routes, we then introduce Off-AIC<sup>2</sup> (Alg. 2), which realizes efficient and incentive-aware offline contracts between ESs and AgPs, inspired by double auction mechanisms in distributed markets [22].

**Step 1. List generation and pivotal-index search.** Off-AIC<sup>2</sup> starts as a sealed-bid, private, and collusion-free mechanism, where all ES buyers  $s_i$  and AgP sellers  $s_k$  simultaneously submit their bids and asks to the auctioneer. We first sort participants to align the bid-ask hierarchy: ESs are ordered into a list  $\mathcal{L}^{\text{ES}}$  by descending average bid  $\overline{\text{bid}}_i$ , and AgPs are ordered into a list  $\mathcal{L}^{\text{AgP}}$  by ascending ask price  $\text{ask}_k$ . Without loss of generality, we relabel indices so that these sorted orders are reflected directly by  $i$  and  $k$ . Then, the algorithm searches for a pair of *pivotal ranks*  $(I^*, K^*)$  such that the cumulative capacity of the top- $K^*$  AgPs can cover the aggregate demand of the top- $I^*$  ESs under a feasible price relationship as  $\overline{\text{bid}}_{I^*} \geq \text{ask}_{K^*}$ ,  $\sum_{k=1}^{K^*} C_k^{\text{V}} \geq \sum_{i=1}^{I^*} N_i^{\text{Dem}}$ . Intuitively,  $(I^*, K^*)$  identifies a largest feasible trading region where high-bidding ESs are matched with low-asking AgPs, and the selected AgPs have sufficient aggregate capacity to serve the selected ESs, thus laying the foundation for near-clearing and budget-balanced trading under current market conditions.

**Step 2. ES-AgP matching and route planning via eACO-VRP.** Given the pivotal ranks  $(I^*, K^*)$ , only the top- $I^*$  ESs and top- $K^*$  AgPs proceed to the matching stage. We initialize the set of *unmatched* ESs as  $\mathcal{U}^{\text{free}} = \{1, \dots, I^*\}$  and iterate over AgP sellers  $s_k$  in the order of  $\mathcal{L}^{\text{AgP}}$ . For each  $s_k$  with remaining capacity  $C_k^{\text{V}} > 0$  and  $\mathcal{U}^{\text{free}} \neq \emptyset$ , we construct a candidate ES set  $C_k = \{s_i \in \mathcal{U}^{\text{free}} \mid U_{i,k} > 0, \text{bid}_{i,k} \geq \overline{\text{bid}}_i\}$ , where  $U_{i,k} = \text{bid}_{i,k} - \text{ask}_k$  denotes the marginal utility of serving ES  $s_i$  with AgP  $v_k$ . Then,  $v_k$  invokes the eACO-VRP (see Alg. 1), which explicitly incorporates the individual information of ESs and AgPs, such as ES demand volumes and time windows,

---

### Algorithm 2: Proposed Off-AIC<sup>2</sup>

---

- 1 **Input:** ESs  $\mathcal{S}$  with demands  $\{N_i^{\text{Dem}}\}$  and bid matrix  $\{\text{bid}_{i,k}\}$ ; AgPs  $\mathcal{V}$  with asks  $\{\text{ask}_k\}$  and capacities  $\{C_k^{\text{V}}\}$ ; auxiliary info  $\{\text{a}_i, \text{d}_k, \text{r}_k\}$ ; parameter  $\mu$ .
- 2 **Initialization:** Compute per-ES reference bids  $\overline{\text{bid}}_i \leftarrow \text{mean}_k(\text{bid}_{i,k})$ ;
- 3 Utility matrix  $U_{i,k} \leftarrow \text{bid}_{i,k} - \text{ask}_k$ ;
- 4 Set  $\mathbf{X}^* \leftarrow \mathbf{0}$ ,  $\mathbf{p}^{\text{b}*} \leftarrow \mathbf{0}$ ,  $\mathbf{r}^{\text{S}*} \leftarrow \mathbf{0}$ .
- 5 **# Phase 1: List generation & pivotal-rank search**
- 6 Sort ES indices into  $\mathcal{L}^{\text{ES}}$  by  $\overline{\text{bid}}_i$  (desc),
- 7 and AgP indices into  $\mathcal{L}^{\text{AgP}}$  by  $\text{ask}_k$  (asc); relabel  $(i, k)$  accordingly.
- 8 Find a pair of pivotal ranks  $(I^*, K^*)$  such that  $\overline{\text{bid}}_{I^*} \geq \text{ask}_{K^*}$ ,  $\sum_{k=1}^{K^*} C_k^{\text{V}} \geq \sum_{i=1}^{I^*} N_i^{\text{Dem}}$ , and  $I^*$  is maximized (breaking ties by larger capacity slack  $\sum_{k=1}^{K^*} C_k^{\text{V}} - \sum_{i=1}^{I^*} N_i^{\text{Dem}}$ ).
- 9 **# Phase 2: ES-AgP matching**
- 10 Initialize the set of unmatched ESs:  $\mathcal{U}^{\text{free}} \leftarrow \{i \mid 1 \leq i \leq I^*\}$ .
- 11 **for**  $k$  in top- $K^*$  AgPs (according to  $\mathcal{L}^{\text{AgP}}$ ) **do**
- 12     **if**  $C_k^{\text{V}} \leq 0$  **or**  $\mathcal{U}^{\text{free}} = \emptyset$  **then**
- 13         **continue**
- 14     Build candidate ES set
- 15      $C_k \leftarrow \{i \in \mathcal{U}^{\text{free}} \mid U_{i,k} > 0 \wedge \text{bid}_{i,k} \geq \overline{\text{bid}}_i\}$ ;
- 16     **if**  $C_k = \emptyset$  **then**
- 17         **continue**
- 18      $\mathcal{K}_k^* \leftarrow$  Alg. 1 (eACO-VRP) with input  $(C_k, \{N_i^{\text{Dem}}\}_{i \in C_k}, C_k^{\text{V}})$ ;
- 19     **for**  $i \in \mathcal{K}_k^*$  **do**
- 20         Set  $x_{i,k}^{\text{Off}} \leftarrow 1$ ;
- 21         Remove  $i$  from  $\mathcal{U}^{\text{free}}$ :  $\mathcal{U}^{\text{free}} \leftarrow \mathcal{U}^{\text{free}} \setminus \{i\}$ ;
- 22     Update remaining capacity:  $C_k^{\text{V}} \leftarrow C_k^{\text{V}} - \sum_{i \in \mathcal{K}_k^*} N_i^{\text{Dem}}$ .
- 23 Denote the resulting matching by  $\mathbf{X}^*$ .
- 24 **# Phase 3: Pricing via monotone binary search (contract determination)**
- 25 (*ES-side payments*)
- 26 **for** each matched ES  $i$  with  $\sum_k x_{i,k}^{\text{Off}} = 1$  **do**
- 27     Set  $\text{high} \leftarrow \overline{\text{bid}}_i$ ,  $\text{low} \leftarrow \overline{\text{bid}}_{i^*+1}$  (or a safe reserve);
- 28     Let  $b_i^{\text{eff}} \leftarrow \overline{\text{bid}}_i$  be ES  $i$ 's effective bid parameter.
- 29     **while**  $\text{low} < \text{high}$  **do**
- 30         Temporarily set  $b_i^{\text{eff}} \leftarrow (\text{low} + \text{high})/2$ ;
- 31         Rerun Phase 2 on the top- $I^*$  ESs and top- $K^*$  AgPs (using  $b_i^{\text{eff}}$  for ES  $i$ ) to obtain  $\mathbf{X}^{\text{Temp}}$ ;
- 32         **if**  $\sum_k x_{i,k}^{\text{Temp}} = 1$  **then**  $\text{high} \leftarrow b_i^{\text{eff}}$ ;
- 33         **else**  $\text{low} \leftarrow b_i^{\text{eff}}$ ;
- 34     Set  $p_i^{\text{b}*} \leftarrow \text{high}$ .
- 35 (*AgP-side rewards*)
- 36 **for** each matched AgP  $k$  with  $\sum_i x_{i,k}^{\text{Off}} \geq 1$  **do**
- 37     Set  $\text{high} \leftarrow \text{ask}_k$ ,  $\text{low} \leftarrow \text{ask}_{K^*+1}$  (or a safe reserve);
- 38     **while**  $\text{low} < \text{high}$  **do**
- 39         Temporarily set  $\text{ask}_k^{\text{eff}} \leftarrow (\text{low} + \text{high})/2$ ;
- 40         Rerun Phase 2 with  $\text{ask}_k^{\text{eff}}$  to obtain  $\mathbf{X}^{\text{Temp}}$ ;
- 41         **if**  $\sum_i x_{i,k}^{\text{Temp}} \geq 1$  **then**  $\text{low} \leftarrow \text{ask}_k^{\text{eff}}$ ;
- 42         **else**  $\text{high} \leftarrow \text{ask}_k^{\text{eff}}$ ;
- 43     Set  $r_k^{\text{S}*} \leftarrow \text{low}$ .
- 44 **Output:** Matching  $\mathbf{X}^* = \{x_{i,k}^{\text{Off}}\}$ , payments  $\mathbf{p}^{\text{b}*}$ , rewards  $\mathbf{r}^{\text{S}*}$ .

---

travel time and energy cost between ESs, and the payment that  $v_k$  can receive, to jointly determine: (i) which ESs in  $C_k$  to serve within its residual capacity, and (ii) in what visiting order they should be placed along a feasible route. By maximizing the AgP's utility along the constructed route, Alg. 1 outputs a selected ES set  $\mathcal{K}_k^* \subseteq C_k$  and the associated pre-planned path for AgP  $v_k$ . For every  $s_i \in \mathcal{K}_k^*$ , we set  $x_{i,k}^{\text{Off}} = 1$  and remove  $s_i$  from  $\mathcal{U}^{\text{free}}$ , ensuring that each ES is matched to at most one AgP. Stacking the decisions across all AgPs yields the

assignment matrix  $\mathbf{X}^*$ . Moreover, by enforcing  $\text{bid}_{i,k} \geq \overline{\text{bid}}_i$  for all successful pairs  $(s_i, s_k)$ , the matching stage respects ES-side individual rationality.

**Step 3. Pricing and contract finalization via binary search.** Once  $\mathbf{X}^*$  is obtained, Off-AIC<sup>2</sup> determines ES payments and AgP rewards via a monotone binary-search procedure designed to approximate truthfulness and budget balance. For each matched ES buyer  $s_i$  (with  $\sum_k x_{i,k}^{\text{Off}} = 1$ ), we treat  $\text{bid}_i$  as an *effective bid parameter* and iteratively search within  $[\overline{\text{bid}}_{i^*+1}, \overline{\text{bid}}_i]$  to find the minimal critical payment  $p_i^{b^*}$  that keeps  $s_i$  in the winning set when Phase 2 is re-executed under this effective bid. Symmetrically, for each matched AgP seller  $s_k$  (with  $\sum_i x_{i,k}^{\text{Off}} \geq 1$ ), we adjust its effective ask within  $[\text{ask}_{K^*+1}, \text{ask}_k]$  and re-run Phase 2 to determine the maximal acceptable reward  $r_k^{s^*}$  that still preserves its winning status. The resulting settlement vectors  $(\mathbf{p}^{b^*}, \mathbf{r}^{s^*})$  finalize the contracts between ESs and AgPs, leading to fair and incentive-aware trading outcomes under the proposed Off-AIC<sup>2</sup>.

#### D. Explainability and Effectiveness Analysis (e.g., From the View of Auction Properties)

Here, we discuss the fundamental properties that underpin the design of auction in offline stage [14], [22].

**Definition 1. (Individual Rationality)** An auction is said to be *individually rational* if the payment made by any winning ES (to its matched AgP) does not exceed its bid, and the revenue obtained by any winning AgP is no less than its asked price.

**Definition 2. (Truthfulness)** An auction is *truthful* (or *incentive-compatible*) if all ESs and AgPs report their bids and asked prices according to their true private valuations; that is, no participant can benefit from misreporting its information.

**Definition 3. (Budget Balance)** An auction satisfies *budget balance* if the total payment collected from all winning ESs is no less than the total payment made to all winning AgPs.

The proposed offline stage is shown to meet all the above properties, with detailed theoretical analysis and proofs moved to Appx. C due to space limitations.

### V. ONLINE STAGE: POTENTIAL GAME FOR SERVICE SCHEDULING OVER HUMAN-MACHINE ECOSYSTEM

Facing real-time demand from both HuUs and MaUs covered by ESs, we now turn to an online stage, for which we consider two types of players: (i) SPs (e.g., ESs and AgPs), collected as  $\mathcal{S}^{\text{On}} = \{s_1^{\text{On}}, \dots, s_i^{\text{On}}, \dots, s_{|\mathcal{S}^{\text{On}}|}^{\text{On}}\}$ ; and (ii) SDs (e.g., HuUs and MaUs), collected as  $\mathcal{U}^{\text{On}} = \{u_1^{\text{On}}, \dots, u_j^{\text{On}}, \dots, u_{|\mathcal{U}^{\text{On}}|}^{\text{On}}\}$ . In this stage, each SD strategically decides whether to execute tasks locally or offload them to one of the available SPs, while SPs allocate their limited computing capacities among the associated tasks. Such mutually coupled decisions are modeled as a game-theoretic scheduling problem.

To represent the decision of  $u_j^{\text{On}}$ , we define the binary indicator vector

$$\mathbf{X}_j^{\text{On}} = (x_{j,1}^{\text{On}}, x_{j,1}^{\text{On}}, \dots, x_{j,i}^{\text{On}}, \dots, x_{j,|\mathcal{S}^{\text{On}}|}^{\text{On}}) \in \{0, 1\}^{1+|\mathcal{S}^{\text{On}}|}, \quad (9)$$

where  $x_{j,i}^{\text{On}} = 1$  indicates local execution at  $u_j^{\text{On}}$ , and  $x_{j,i}^{\text{On}} = 1$  indicates offloading to provider  $s_i^{\text{On}}$ , with  $x_{j,i}^{\text{On}} \in \{0, 1\}$  and  $x_{j,i}^{\text{On}} \in \{0, 1\}$  for all  $u_j^{\text{On}}$ .

Since each task is either executed locally or offloaded to exactly one SP, we have

$$x_j^{\text{On}} + \sum_{i=1}^{|\mathcal{S}^{\text{On}}|} x_{j,i}^{\text{On}} = 1, \quad \forall j \in \{1, \dots, |\mathcal{U}^{\text{On}}|\}. \quad (10)$$

#### A. Utility of SDs and SPs

1) *Delay and Congestion Model:* We consider SP set  $\mathcal{S}^{\text{On}}$  and SD set  $\mathcal{U}^{\text{On}} = \mathcal{U}^{\text{H}} \cup \mathcal{U}^{\text{A}}$ , where  $\mathcal{U}^{\text{H}}$  and  $\mathcal{U}^{\text{A}}$  denote the sets of HuUs and MaUs, respectively. Each SP  $s_i^{\text{On}}$  has a finite computing capacity  $f_i^{\text{On}} > 0$  (CPU cycles/s). When a subset of SDs  $\mathcal{U}_i = \{u_v^{\text{On}} \in \mathcal{U}^{\text{On}} : x_{v,i}^{\text{On}} = 1\}$  simultaneously offload their workload to  $s_i^{\text{On}}$ , we adopt a weighted processor sharing (WPS) rule [13] to capture computing congestion and differentiated service levels.

Each SD  $u_j^{\text{On}}$  associated with  $s_i^{\text{On}}$  is assigned a positive weight  $\gamma_{j,i} > 0$  that reflects service priority, contract tier, or fairness quota. Under WPS, the effective computing rate that  $u_j^{\text{On}}$  receives from  $s_i^{\text{On}}$  is  $\hat{f}_{j,i}^{\text{On}} = f_i^{\text{On}} \frac{\gamma_{j,i}}{\sum_{u_v^{\text{On}} \in \mathcal{U}_i^{\text{On}}} \gamma_{v,i}}$ , and the corresponding edge-side computing delay is

$$t_{j,i}^{\text{comp}} = \frac{r_j}{\hat{f}_{j,i}^{\text{On}}} = \frac{r_j}{\gamma_{j,i}} \times \frac{\sum_{u_v^{\text{On}} \in \mathcal{U}_i^{\text{On}}} \gamma_{v,i}}{f_i^{\text{On}}}, \quad (11)$$

where  $r_j$  denotes the computing workload (e.g., CPU cycles needed) of  $u_j^{\text{On}}$ . This WPS model compactly captures how the delay of each individual SD grows with the aggregate weighted load at the SP.

To facilitate analysis, we then define the *effective congestion load* at  $s_i^{\text{On}}$  as  $y_i = \sum_{u_v^{\text{On}} \in \mathcal{U}_i^{\text{On}}} \gamma_{v,i}$ , so that (11) can be written in a factorized form as

$$t_{j,i}^{\text{comp}} = \theta_{j,i} \tau_i(y_i), \quad \theta_{j,i} = \frac{r_j}{\gamma_{j,i}}, \quad \tau_i(y) = \frac{y}{f_i^{\text{On}}}. \quad (12)$$

where  $\theta_{j,i}$  is a user-specific load factor, whereas  $\tau_i(y)$  captures the server-side congestion effect as a function of the aggregate load. This separable structure will be instrumental for constructing an ordinal potential in the subsequent analysis. In addition, when  $u_j^{\text{On}}$  offloads to  $s_i^{\text{On}}$ , the uplink transmission delay is given by  $t_{j,i}^{\text{tx}} = \frac{d_j}{W \log_2(1 + e_j^{\text{tx}} \Gamma_{j,i})}$ , where  $d_j$  is the input data size,

$W$  is the communication bandwidth,  $e_j^{\text{tx}}$  is the transmit power, and  $\Gamma_{j,i}$  is the SNR-related channel gain between  $u_j^{\text{On}}$  and  $s_i^{\text{On}}$ . The total edge-side latency experienced by  $u_j^{\text{On}}$  when uploading its workload to  $s_i^{\text{On}}$  is then

$$T_{j,i}^{\text{edge}} = t_{j,i}^{\text{comp}} + t_{j,i}^{\text{tx}}. \quad (13)$$

2) *Utility of HuUs:* Consider a HuU  $u_j^{\text{On}} \in \mathcal{U}^{\text{H}}$  with local CPU frequency  $f_j^{\text{loc}}$  and local energy coefficient  $e_j^{\text{loc}}$ . The local execution time and energy consumption of its task are  $t_j^{\text{loc}} = \frac{r_j}{f_j^{\text{loc}}}$  and  $E_j^{\text{loc}} = \frac{r_j e_j^{\text{loc}}}{f_j^{\text{loc}}}$ . By transferring its task to  $s_i^{\text{On}}$ , the HuU achieves a latency saving  $t_{j,i}^{\text{save}} = t_j^{\text{loc}} - (t_{j,i}^{\text{comp}} + t_{j,i}^{\text{tx}})$ , and an energy saving  $c_{j,i}^{\text{save}} = E_j^{\text{loc}} - E_{j,i}^{\text{tx}}$ , where  $E_{j,i}^{\text{tx}}$  denotes the uplink transmission energy.

We introduce non-negative valuation coefficients  $\mathbb{V}_t^{\text{H}}$  and  $\mathbb{V}_e^{\text{H}}$  to capture HuU sensitivities to latency and energy, respectively. The HuU's perceived valuation of being served by  $s_i^{\text{On}}$  is

modeled as  $v_{j,i}^H = \mathbb{V}_t^H t_{j,i}^{\text{save}} + \mathbb{V}_e^H c_{j,i}^{\text{save}}$ . If  $s_i^{\text{On}}$  charges a price  $p_{j,i}$  for serving  $u_j^{\text{On}}$ , the HuU's utility becomes

$$U_{j,i}^H = v_{j,i}^H - p_{j,i}, \quad U_{j,0}^H = 0, \quad (14)$$

where  $U_{j,0}^H$  corresponds to local execution as a baseline.

3) *Utility of MaUs*: An MaU  $u_j^{\text{On}} \in \mathcal{U}^A$  is associated with a latency deadline  $D_j > 0$ . Its total edge-side latency at  $s_i^{\text{On}}$  is  $T_{j,i}^{\text{edge}}$  in (13). To model their deadline-aware behavior,

we adopt a soft-deadline valuation as  $G_{j,i}^A = v_j \frac{[D_j - T_{j,i}^{\text{edge}}]_+}{D_j}$ , where  $[x]_+ = \max\{x, 0\}$ , and  $v_j > 0$  is the MaU's task reward. Intuitively, the MaU only accrues reward when the deadline is met, while partial lateness leads to a proportional loss of reward. Similar to HuUs, the MaU's energy saving from enjoying edge services is  $c_{j,i}^{\text{A,save}} = E_j^{\text{loc}} - E_{j,i}^{\text{tx}}$ . Let  $\mathbb{V}_e^A$  refer to MaU's valuation coefficient on energy saving. MaU's utility is given by

$$U_{j,i}^A = G_{j,i}^A + \mathbb{V}_e^A c_{j,i}^{\text{A,save}} - p_{j,i}, \quad U_{j,0}^A = 0. \quad (15)$$

Note that both HuU and MaU utilities in (14) and (15) share the same congestion component  $t_{j,i}^{\text{comp}} = \theta_{j,i} \tau_i(y_i)$  in (12). This common structure is pivotal for constructing an ordinal potential function that aligns individual incentives with system-wide performance in the next subsection.

4) *Cost of SP*: For SP  $s_i^{\text{On}}$ , the aggregate computing load induced by its associated users is  $\mathbb{x}_i = \sum_{u_j^{\text{On}} \in \mathcal{U}_i^{\text{On}}} r_j$ . We model the SP-side computation/operation cost as  $K_i(\mathbb{x}_i) = \omega_1 e_i^{\text{comp}} \frac{\mathbb{x}_i}{f_i^{\text{On}}} + \omega_2 c_i^{\text{hard}}$ , where  $e_i^{\text{comp}}$  is the average computing power consumption of  $s_i^{\text{On}}$ . Although a SP may collect service payments  $\sum_{u_j^{\text{On}} \in \mathcal{U}_i^{\text{On}}} p_{j,i}$ , these payments are pure monetary transfers among agents and therefore cancel out when aggregating the system-level welfare. Consequently, they do not appear in the potential function constructed later and only affect how the welfare is divided among participants rather than the overall efficiency.

## B. Ordinal Potential Function

We construct an *ordinal potential* [13], [20] for the online game under the soft-deadline utilities of MaUs, leveraging the unified congestion structure established above. The key observation is that all users (HuUs and MaUs) experience congestion through the same factorized computing delay as (12). Then, for MaU  $u_j^{\text{On}}$  assigned to  $s_i^{\text{On}}$ , the soft-deadline valuation is

$$G_{j,i}^A = v_j \frac{[D_j - (t_{j,i}^{\text{comp}} + t_{j,i}^{\text{tx}})]_+}{D_j}, \quad [x]_+ = \max\{x, 0\}. \quad (16)$$

Since  $t_{j,i}^{\text{comp}}$  in (12) is increasing in  $y_i$ , heavier congestion directly reduces  $G_{j,i}^A$ . In other words, load accumulation at a SP gradually erodes the MaU's reward for meeting its deadline.

For HuUs, the utility in (14) can be decomposed into a congestion-independent part and a congestion-dependent penalty, given by

$$U_{j,i}^H = \underbrace{\mathbb{V}_t^H (t_{j,i}^{\text{loc}} - t_{j,i}^{\text{tx}})}_{S_j(i) \text{ (independent of } y_i)} + \underbrace{\mathbb{V}_e^H (E_j^{\text{loc}} - E_{j,i}^{\text{tx}})}_{\text{congestion penalty}} - \mathbb{V}_t^H \theta_{j,i} \tau_i(y_i) - p_{j,i}. \quad (17)$$

where  $S_j(i)$  collects all terms that do not depend on the congestion load  $y_i$ , while the second term captures how queueing-induced delay degrades HuU utility.

Under soft deadlines, MaU utilities admit the same structural form. By linearizing  $G_{j,i}^A$  around typical delay levels (see Appx. D-D), the MaU utility can be rewritten as

$$U_{j,i}^A = \bar{S}_j(i) - \kappa_j \theta_{j,i} \tau_i(y_i) - p_{j,i}, \quad (18)$$

where  $\bar{S}_j(i)$  collects the non-congestion terms (soft-deadline base reward and energy saving), and  $\kappa_j > 0$  reflects the MaU's effective sensitivity to congestion. This linearized form is standard in congestion and potential-game analysis and preserves the ordinal structure of preferences, even if the original soft-deadline utility is mildly nonlinear.

Considering HuUs and MaUs, the utility of SD  $u_j^{\text{On}} \in \mathcal{U}^{\text{On}}$  taking action  $\mathcal{X}^{\text{On}} \in \{0, 1\}$  can be unified as

$$U_{j,i} = S_j(i) - \kappa_j \theta_{j,i} \tau_i(y_i) - p_{j,i}, \quad (19)$$

where  $S_j(0) = 0$ , and where  $\tau_i(\cdot)$  is relevant only for  $i \in \mathcal{S}^{\text{On}}$  (local execution does not suffer edge-side congestion). This unified form makes explicit that all heterogeneity is captured by user-specific coefficients ( $S_j, \kappa_j, \theta_{j,i}$ ) on top of a shared congestion mechanism.

Let  $\pi = (\pi_j)_{j \in \mathcal{U}^{\text{On}}}$  denote the joint assignment profile, where  $\pi_j \in \{0\} \cup \mathcal{S}^{\text{On}}$  and  $\pi_j = 0$  stands for local execution, while  $\pi_j = i$  means offloading to  $s_i^{\text{On}}$ . Given  $\pi$ , the effective congestion load and the physical computing load at  $s_i^{\text{On}}$  are

$$y_i(\pi) = \sum_{j: \pi_j = i} \gamma_{j,i}, \quad \mathbb{x}_i(\pi) = \sum_{j: \pi_j = i} r_j, \quad (20)$$

which drive, respectively, the delay inflation via  $\tau_i(\cdot)$  and the SP-side cost via  $K_i(\cdot)$ .

Thus, we define the following potential function:

$$\begin{aligned} \Phi(\pi) = & \underbrace{\sum_{j: \pi_j \neq 0} S_j(\pi_j)}_{\text{user-side non-congestion benefits}} \\ & - \underbrace{\sum_{i \in \mathcal{S}^{\text{On}}} \int_0^{y_i(\pi)} \tau_i(z) dz}_{\text{integrated time-congestion cost}} - \underbrace{\sum_{i \in \mathcal{S}^{\text{On}}} K_i(\mathbb{x}_i(\pi))}_{\text{SP computation/operation cost}}. \end{aligned} \quad (21)$$

where, the first term aggregates all non-congestion benefits obtained by users that offload to the edge. The second term integrates the congestion function  $\tau_i(\cdot)$  from zero to the realized load  $y_i(\pi)$ , and thus acts as a ‘‘convex penalty’’ for overloading SPs. Under the linear response  $\tau_i(y) = y/f_i^{\text{On}}$ , this integral simplifies to  $y_i^2(\pi)/(2f_i^{\text{On}})$ , which is strictly convex in  $y_i$ . The last term accounts for SP-side computing and operational costs, ensuring that the potential internalizes both SD-side and SP-side effects.

Consider a unilateral deviation where exactly one SD switches from SP  $s_i^{\text{On}}$  to SP  $s_i^{\text{On}}$  (or to local execution). The change in  $\Phi(\pi)$  has three components:

- The increment in the first term of (21) equals the change in that SD's non-congestion benefit,  $S_j(\cdot)$ .
- The increment in the second term is determined by the difference between the integrated congestion before and after the deviation. Since  $\tau_i(\cdot)$  is increasing, this difference has the same sign as the change in that SD's individual congestion penalty,  $\kappa_j \theta_{j,i} \tau_i(y_i)$ , up to a scalar factor; this is a standard ‘‘integral–pointwise sandwich’’ argument in congestion games.

- The increment in the third term reflects SP-side cost variation due to the convexity of  $K_i(\cdot)$  w.r.t. the physical load  $x_i(\pi)$ .

Therefore, whenever a SD changes its action in a way that strictly increases its own utility (disregarding pure payment transfers), the induced change in  $\Phi(\pi)$  has the same sign. In this sense,  $\Phi(\pi)$  serves as an *ordinal potential* under the soft-deadline setting<sup>5</sup>.

### C. Properties of the Ordinal Potential

We now formalize  $\Phi(\pi)$  in (21) as an ordinal potential for the online game under soft-deadline utilities. The proof follows a standard single-user deviation argument and relies on three ingredients: (i) separability of non-congestion terms  $S_j(\cdot)$ , (ii) a sandwich bound connecting the *pointwise* congestion penalty in user utilities with the *integrated* congestion cost in  $\Phi(\pi)$ , and (iii) monotonicity/convexity of the SP-side cost  $K_i(\cdot)$ . Full details are moved to Appendices D-C-D-G.

**Theorem 1** (Ordinal potential). *Consider utilities in (19) with soft-deadline MaUs and the potential  $\Phi(\pi)$  in (21). For any SD  $u_j^{\text{On}}$  and any unilateral deviation  $\pi_j = \hat{i} \rightarrow \hat{i}'$ , if  $U_{j,\hat{i}'} - U_{j,\hat{i}} > 0$ , then  $\Phi(\pi_{-j}, \hat{i}') - \Phi(\pi_{-j}, \hat{i}) > 0$ . Hence,  $\Phi(\pi)$  is an ordinal potential for the considered game [13].*

Since each SD possesses a finite action set, any sequence of unilateral best-response updates yields a strictly increasing trajectory of the potential function  $\Phi(\pi)$  and therefore converges in finitely many iterations to a pure-strategy NE. Consequently, every local maximizer of  $\Phi(\pi)$  corresponds to a pure-strategy NE. A formal proof is provided in Appx. D-H.

### D. Problem Formulation

In this online stage, we use ordinal potential  $\Phi(\pi)$  in (21) as a system-level surrogate to coordinate heterogeneous SDs and SPs. Since any unilateral utility-improving move strictly increases  $\Phi(\pi)$  (Theorem 1), any maximizer of  $\Phi(\pi)$  corresponds to a pure-strategy NE that balances user-side benefits and SP-side costs under congestion. The resulting design can be cast as the following optimization problem  $\mathcal{F}^{\text{II}}$ :

$$\mathcal{F}^{\text{II}}: \quad \underset{\pi}{\operatorname{argmax}} \quad \Phi(\pi) \quad (22)$$

$$\text{s.t. } \pi_j \in \{0\} \cup \mathcal{S}^{\text{On}}, \quad \forall u_j^{\text{On}} \in \mathcal{U}^{\text{On}} \quad (22a)$$

$$x_{j,\hat{i}}^{\text{On}} = 0, \text{ if } s_{\hat{i}}^{\text{On}} \notin \mathcal{C}_{\hat{i}}, \quad \forall u_j^{\text{On}} \in \mathcal{U}^{\text{On}} \quad (22b)$$

$$\sum_{u_j^{\text{On}} \in \mathcal{U}^{\text{On}}} x_{j,\hat{i}}^{\text{On}} \leq G_{\hat{i}}, \quad \forall s_{\hat{i}}^{\text{On}} \in \mathcal{S}^{\text{On}} \quad (22c)$$

where  $\pi = (\pi_j)_{j \in \mathcal{U}^{\text{On}}}$  represents the joint scheduling strategy; constraint (22a) enforces that each SD chooses either local execution or exactly one SP; constraint (22b) encodes the service-coverage feasibility condition: any SD located outside the service region of SP  $u_j$ , is ineligible for assignment. constraint (22c) ensures that the number of SDs served by each SP does not exceed its maximum access  $G_{\hat{i}}$ .

Problem  $\mathcal{F}^{\text{II}}$  represents a finite mixed-integer programming (MIP) problem over a discrete action space and is, in general,

<sup>5</sup>Payment terms  $p_{j,\hat{i}}$  are pure monetary transfers between SPs and SDs, and are excluded from  $\Phi(\pi)$ ; they affect the distribution of SW but not the total SW. A short justification is provided in Appx. D-I.

### Algorithm 3: Proposed PG-BRD

---

```

1 Input:  $\mathcal{U}^{\text{On}}$ ,  $\mathcal{S}^{\text{On}}$ , and max iterations  $T_{\max}$ .
2 Initialization: Randomly construct an initial feasible profile
    $\pi^{(0)} = (\pi_j^{(0)})_{j \in \mathcal{U}^{\text{On}}}$  such that constraints (22a)–(22c) are satisfied,
   set  $t \leftarrow 0$ 
3 while not converged and  $t < T_{\max}$  do
4   For each SP  $s_{\hat{i}}^{\text{On}} \in \mathcal{S}^{\text{On}}$ , compute  $y_{\hat{i}}(\pi^{(t)})$ ,  $x_{\hat{i}}(\pi^{(t)})$ , and
      $n_{\hat{i}}(\pi^{(t)})$ .
5   generate a random permutation of  $\mathcal{U}^{\text{On}}$ .
6   for each SD  $u_j^{\text{On}}$  in the permutation do
7     let  $a_j^{\text{cur}} = \pi_j^{(t)}$ ; for all  $\hat{i}$ , obtain  $y_{\hat{i}}^{-j}$ ,  $x_{\hat{i}}^{-j}$ ,  $n_{\hat{i}}^{-j}$ 
8     build  $\mathcal{A}_j^{\text{feas}}$  according to (23).
9     compute current utility  $U_j(a_j^{\text{cur}} | \pi_{-j}^{(t)})$  via (19);
10    for each  $a \in \mathcal{A}_j^{\text{feas}}$ , form hypothetical loads  $y_{\hat{i}}^{(j \rightarrow a)}$ ,
       $x_{\hat{i}}^{(j \rightarrow a)}$  and evaluate  $U_j(a | \pi_{-j}^{(t)})$ ;
11    let  $a_j^{\text{best}} \in \arg \max_{a \in \mathcal{A}_j^{\text{feas}}} U_j(a | \pi_{-j}^{(t)})$ .
12    if  $U_j(a_j^{\text{best}} | \pi_{-j}^{(t)}) - U_j(a_j^{\text{cur}} | \pi_{-j}^{(t)}) > \varepsilon$  then
13      | set  $\pi_j^{(t+1)} \leftarrow a_j^{\text{best}}$ 
14    else
15      | set  $\pi_j^{(t+1)} \leftarrow \pi_j^{(t)}$ 
16    if no SD updates its action in this pass, declare convergence;
17     $t \leftarrow t + 1$ .
18 Output: NE profile  $\pi^*$  (final  $\pi^{(t)}$ ) and the associated allocation.
```

---

NP-hard. Instead of attempting global optimization, Theorem 1 guarantees that distributed better/best-response dynamics, where each SD myopically maximizes its own utility subject to feasibility, monotonically increase  $\Phi(\pi)$  and converge in finitely many steps to a pure-strategy NE, which serves as a local optimal solution to (22) with provable convergence and low online complexity.

### E. Potential-Guided Best-Response Dynamics (PG-BRD)

We consider an online ordinal-potential game among SDs and SPs under the hard coverage and subcarrier-capacity constraints in (22b)–(22c). Each SD myopically updates its decision to maximize its own utility, while the underlying ordinal potential  $\Phi(\pi)$  guarantees convergence to a pure-strategy NE.

**Step 1. Random-feasible initialization.** We first construct a random feasible association profile  $\pi^{(0)} \in \{0, 1, \dots, |\mathcal{S}^{\text{On}}|\}^{|\mathcal{U}^{\text{On}}|}$ , where  $\pi_j = 0$  corresponds to local execution and  $\pi_j = \hat{i} > 0$  corresponds to transferring task data to SP  $s_{\hat{i}}^{\text{On}}$ . For each SD  $u_j^{\text{On}}$ , we randomly select an action from  $\{0\} \cup \mathcal{C}_j$  such that the resulting profile satisfies the coverage/access constraint (22b) and the subcarrier constraint (22c). This random-feasible initialization avoids starting from an infeasible point and provides a diverse baseline for the subsequent best-response updates.

**Step 2. Feasible-action enumeration under coverage and subcarrier caps.** Given the current profile  $\pi$ , we compute for each SP  $s_{\hat{i}}^{\text{On}}$  the effective congestion load  $y_{\hat{i}}(\pi)$  and the physical computing load  $x_{\hat{i}}(\pi)$  as in (20), as well as the number of attached SDs  $n_{\hat{i}}(\pi)$ . When updating a particular SD  $u_j^{\text{On}}$ , we first remove its current contribution, obtaining  $y_{\hat{i}}^{-j}$ ,  $x_{\hat{i}}^{-j}$ , and  $n_{\hat{i}}^{-j}$ . Based on these “others-fixed” loads, we construct the SD’s feasible action set  $\mathcal{A}_j^{\text{feas}}$  as in (23): local execution  $a = 0$  is always feasible, while an offloading action  $a = \hat{i} > 0$  is feasible only if  $s_{\hat{i}}^{\text{On}} \in \mathcal{C}_j$  and the resulting number of served

SDs does not exceed the subcarrier cap, i.e.,  $n_i^{-j} + 1 \leq G_i$ . This step hard-prunes any action that would violate coverage or SP capacity constraints.

**Step 3. Asynchronous best response under the ordinal potential.** We adopt asynchronous updates: at each iteration, SDs are visited in a random order. For a given SD  $u_j^{\text{On}}$  and current profile  $\pi$ , we first evaluate its current utility  $U_j(\pi_j | \pi_{-j})$  according to the unified form in (19). Then, for each feasible action  $a \in \mathcal{A}_j^{\text{feas}}$ , we form the hypothetical congestion and load variables and compute the corresponding utility  $U_j(a | \pi_{-j})$ . The SD selects a best response  $a_j^{\text{best}} \in \arg \max_{a \in \mathcal{A}_j^{\text{feas}}} U_j(a | \pi_{-j})$ . To avoid oscillations caused by marginal improvements, we employ an acceptance threshold  $\varepsilon > 0$ : the SD updates its decision only if

$$U_j(a_j^{\text{best}} | \pi_{-j}) - U_j(\pi_j | \pi_{-j}) > \varepsilon.$$

Otherwise, it keeps  $\pi_j$  unchanged. Because the game admits the ordinal potential  $\Phi(\pi)$ , each accepted update strictly increases  $\Phi(\pi)$ .

**Step 4. Convergence and NE detection.** We repeatedly perform feasible-action enumeration and asynchronous best responses by cycling over all SDs. When a full pass over  $\mathcal{U}^{\text{On}}$  yields no accepted update, no SD can further improve its utility by more than  $\varepsilon$  via a unilateral deviation, and the algorithm has reached a pure-strategy NE  $\pi^*$ . The resulting equilibrium profile  $\pi^*$  serves as a locally optimal solution to problem (22), balancing user-side benefits and SP-side costs under congestion-aware service scheduling.

## VI. EVALUATIONS

This section conducts extensive experiments to evaluate our FUSION, via testing both numerical and real-world datasets on various evaluation metrics..

We consider a square service region of size 1000 m  $\times$  1000 m, where ESs are randomly deployed and act as long-term buyers of computing service enhancement, where AgPs can be dispatched to assist overloaded ESs. The availability windows of ESs are randomly generated over a normalized time horizon to capture the temporal variability of computation demand. For clarity of exposition, ESs are uniformly distributed across the region, whereas HuUs and MaUs are placed within the coverage areas of selected ESs to emulate heterogeneous and spatially clustered service demands. Other key parameters are [22], [25], [29]:  $f_i^E \in [1, 3] \times 10^{12}$  CPU cycles/s,  $f_k^V \in [1, 3] \times 10^{12}$  CPU cycles/s,  $f_m^{\text{H,loc}} = f_n^{\text{A,loc}} \in [1, 2] \times 10^9$  CPU cycles/s,  $d_m^{\text{H}} \in [10, 55]$  Mbit,  $d_n^{\text{A}} \in [100, 550]$  Mbit,  $G_i \in [6, 8]$ ,  $G_k^V \in [1, 2]$ ,  $C_k^V \in [8, 10]$ ,  $W = 50$  MHz,  $e_m^{\text{H,tx}} = e_n^{\text{A,tx}} \in [0.2, 0.4]$  W,  $r_m^{\text{H}} = 600$  cycles/bit  $\times d_m^{\text{H}}$ , and  $r_n^{\text{A}} = 600$  cycles/bit  $\times d_n^{\text{A}}$ . Channel gains are synthesized based on distance-dependent coverage with SNRs uniformly drawn from [10, 25] dB, and UAV links enjoy a 20% SNR boost to capture their better propagation conditions.

To ensure statistical reliability, all figures are obtained via Monte Carlo method, where each data point represents the average result over 100 independent trials.

### A. Benchmark Methods and Evaluation Metrics

We evaluate our FUSION from two complementary angles: (i) prediction performance (regarding offline stage) on service demand forecasting module (Sec. VI-B); and (ii) system-level performance of FUSION (Sec. VI-C).

1) *Benchmarks and Metrics for Demand Forecasting (offline stage)*: We first compare our Pro-LNN module against two widely used prediction models.

- **LSTM-driven demand prediction [27]**: A standard long short-term memory network applied to the same input sequences  $\{z_i\}$ , trained to predict future ES demands. This baseline represents a strong discrete-time RNN.

- **Transformer-driven demand prediction [28]**: A temporal Transformer-based predictor with self-attention over the historical context window. This serves as a powerful high-capacity baseline, but typically requires more parameters and computing resources.

To achieve better evaluations, we consider the following criteria:

- **Accuracy**: We report the root mean square error (RMSE), mean absolute error (MAE), and symmetric mean absolute percentage error (sMAPE) of the  $H$ -step forecasts  $\{\hat{N}_i^{\text{Dem},(v+1:v+H)}\}$  against the ground truth  $\{N_i^{\text{Dem},(v+1:v+H)}\}$ , averaged over all ESs and all test instances.

- **Model footprint**: We measure the total number of trainable parameters and the corresponding FP32 model size (in megabytes) of each predictor, which together characterize its memory and storage requirements on edge devices.

- **Robustness**: To assess robustness under realistic noisy conditions, we compare the mean squared error (MSE) on clean test inputs with that on corrupted inputs containing randomly missing observations, additive perturbations, and occasional demand bursts, and report the resulting performance drop  $\Delta\text{MSE}$ .

2) *System-Level Benchmarks and Metrics (For Comparing With Our FUSION)*: We then compare FUSION with several benchmark methods that modify or simplify either stages, to highlight the benefits of prediction-driven contracting, time-window-aware routing, and potential-based online coordination.

- **Pure online scheduling (PurOnline) [13]**: This baseline removes the offline stage completely, e.g., ESs and AgPs do not sign any offline contracts, and UAV locations are not pre-planned. All HuUs and MaUs directly enter the online market, where their tasks are scheduled only via the PG-BRD-based potential game over the current ES/AgP topology.

- **Two-stage without PG-based online scheduling (FUSION\_NoPG)**: This variant keeps the same offline stage as FUSION, i.e., Off-AIC<sup>2</sup> with eACO-VRP is still used to form offline AgP-ES contracts and pre-planned routes. However, the online stage abandons PG-BRD: HuU/MaU tasks are randomly assigned to feasible ESs/AgPs within coverage, subject to capacity and deadline constraints. This aims to isolate the contribution of the online potential game.

- **Two-stage with random offline contracts (FUSION\_Random)**: Here, an online stage is identical to FUSION and still relies on PG-BRD for congestion-aware online scheduling. In contrast, offline stage no longer uses Off-AIC<sup>2</sup>

---


$$\mathcal{A}_j^{\text{feas}} = \left\{ a \in \{0\} \cup \mathcal{S}^{\text{On}} \mid a = 0 \text{ or } (a = i > 0, s_i^{\text{On}} \in C_j, n_i^{-j} + 1 \leq G_i) \right\}, \quad (23)$$

TABLE II

ROBUSTNESS–COMPLEXITY COMPARISON OF DIFFERENT FORECASTERS ON SYNTHETIC NON-STATIONARY SERIES. THE “CORRUPT” CASE INJECTS 30% RANDOM MISSING VALUES, GAUSSIAN NOISE WITH  $\sigma = 0.05$ , AND RANDOM BURST SHOCKS.

Model	#Params	MSE <sub>clean</sub>	MSE <sub>corrupt</sub>	$\Delta$ MSE	Rel. increase
LSTM	52800	0.119	0.983	0.864	+726.3%
Transformer	69500	0.467	0.781	0.314	+67.3%
Pro-LNN	11100	0.459	0.762	0.303	+66.1%

or eACO-VRP; instead, each AgP is randomly associated with a subset of ESs and moves along a randomly generated feasible route until its capacity is exhausted. This quantifies the gain brought by a well-designed economic and path-aware offline contracting.

• **Two-stage without ES spatio-temporal features (FUSSION\_NoST):** This preserves the two-stage structure, but the offline auction ignores ES-specific time windows and travel-time constraints. AgP–ES pairs are determined only by simple price/volume trading without using eACO-VRP, while online stage still runs PG-BRD for task scheduling. This aims highlighting the benefits of explicitly modeling ES spatio-temporal characteristics during offline stage.

To provide a comprehensive performance assessment, we adopt the following metrics.

• **Social welfare (SW):** The sum of utilities of all ESs, the AgPs, and users across both stages. In the offline stage, SW accounts for ES profits, AgP utilities, and auctioneer surplus as in (1)–(3). Then, during offline stage, it is aligned with the potential value  $\Phi(\pi)$ , which combines SD-side benefits and SP-side costs under congestion.

• **Delay incurred by interactions between SPs and SDs (DoI):** This captures the total decision-making latency (in milliseconds) induced by control-message exchanges between ESs/AgPs (SPs) and HuUs/MaUs (SDs) across both stages. Following [29]–[31], we assume that the per-interaction delay lies in the range of [1, 15] ms, and obtain DoI by multiplying the total number of interactions with the corresponding per-interaction delay.

• **Energy consumption incurred by interactions between SPs and SDs (ECoI):** This metric measures the signaling-related energy consumption (in watts-ms) during the decision-making process. To compute ECoI, we assume that the transmit power of HuUs/MaUs lies in [0.2, 0.4] W, while that of ESs/AgPs lies in [6, 20] W, consistent with [29], [30]. By aggregating the energy consumed by all control-message transmissions under these power levels and the corresponding interaction delays, we obtain the overall ECoI.

• **Truthfulness and individual rationality of Off-AIC<sup>2</sup>:** To empirically verify the theoretical guarantees of Off-AIC<sup>2</sup>, we conduct experiments in which ESs and AgPs are allowed to deviate from their truthful bids/asks. We measure the proportion of agents whose utilities increase under such deviations. An auction that is truthful and individually rational should ensure that (i) every winning ES attains a non-negative utility and cannot benefit from misreporting its bid, and (ii) every winning AgP receives a payment no lower than its declared ask and gains no advantage by inflating or deflating it.

TABLE III

PREDICTION ACCURACY AND MODEL FOOTPRINT ON THE UCI ELECTRICITY LOAD DIAGRAMS 2011–2014 DATASET (FEEDERS MT\_005 AND MT\_145, INPUT LENGTH  $T_{\text{his}} = 48$ , PREDICTION HORIZON  $H = 10$ ).

Model	#Params	Size (MB)	RMSE	MAE	sMAPE
LSTM	52842	0.204	0.1121	0.0816	0.1831
Transformer	69482	0.400	0.1158	0.0824	0.1864
Pro-LNN	11114	0.046	0.1234	0.0906	0.1983

TABLE IV

ROBUSTNESS TO MISSING AND NOISY INPUTS ON UCI ELECTRICITY (30% RANDOM MISSING, GAUSSIAN NOISE WITH STANDARD DEVIATION 0.05, BURST PROBABILITY 0.2).

Model	MSE (clean)	MSE (corrupt)	$\Delta$ MSE
LSTM	0.0126	0.0485	0.0359
Transformer	0.0134	0.0592	0.0458
Pro-LNN	0.0152	0.0467	0.0315

## B. Prediction Performance Evaluation

1) *Robustness vs. Cost:* We first conduct experiments on “robustness vs. cost”, regarding synthetic non-stationary time series, summarized by Table II. The “clean” setting feeds each model with intact historical sequences, while the “corrupt” setting injects 30% random missing values, additive Gaussian noise with standard deviation  $\sigma = 0.05$ , and random burst shocks of length 1–3. On clean data, LSTM attains the lowest MSE (0.119), whereas Transformer and Pro-LNN yield slightly larger errors (0.467 and 0.459, respectively). This gap is expected, as LSTM and Transformer contain approximately 52.8k and 69.5k parameters, compared to only 11.1k parameters for Pro-LNN, implying significantly higher computational and memory costs. Once input corruptions are introduced, however, LSTM error surges to 0.983 (a relative increase of +726.3%), while the errors of Transformer and Pro-LNN only grow to 0.781 and 0.762 (relative increases of +67.3% and +66.1%), respectively. These results indicate that Pro-LNN offers a more favorable trade-off between robustness and cost than an over-parameterized LSTM on highly non-stationary and noisy sequences, which matches the characteristics of ES demand trajectories in Off-AIC<sup>2</sup>.

2) *Real-world Dataset Test:* We then validate our Pro-LNN on real-world UCI Electricity Load Diagrams 2011–2014 dataset [32], using two representative feeders (MT\_005 and MT\_145). We construct a univariate forecasting task where a history of  $T_{\text{his}} = 48$  measurements is used to predict the next  $H = 10$  time steps. These forecasts can be viewed as a proxy for the future aggregate demand of ESs for our Off-AIC<sup>2</sup>, since electricity loads and ES demands share similar temporal patterns such as diurnal cycles and bursty fluctuations. Quantitative results are summarized in Table III and Table IV.

Observing Table III, Pro-LNN achieves comparable prediction accuracy to LSTM and Transformer, while being much more compact. In particular, Pro-LNN attains an RMSE of 0.1234, close to that of the LSTM (0.1121) and the Transformer (0.1158), but only uses 11,114 parameters and a 0.046 MB footprint. This corresponds to roughly 4–6 $\times$  fewer parameters and 4–9 $\times$  smaller model size than the two benchmark methods, making our Pro-LNN highly attractive for deployment on resource-constrained edge networks.

To evaluate robustness on real data, we inject realistic input corruptions into the test set, including 30% randomly

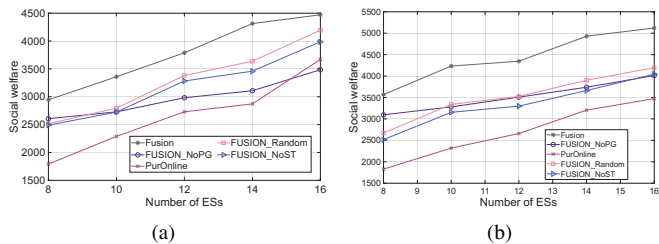


Fig. 2. Performance comparisons in terms of SW. We consider 80 HuUs, 80 MaUs, and 5 AgPs in (a), and 90 HuUs, 90 MaUs, and 7 AgPs in (b).

missing observations, additive Gaussian noise with standard deviation 0.05, and occasional bursty spikes with probability 0.2. As reported in Table IV, Pro-LNN exhibits the smallest performance degradation among all models: its MSE increases from 0.0152 (clean) to 0.0467 (corrupt), yielding a  $\Delta$ MSE of 0.0315, which is lower than that of both LSTM (0.0359) and Transformer (0.0458). These observations indicate that Pro-LNN is highly parameter-efficient and demonstrates strong robustness to missing data and measurement noise in real-world electricity load traces.

Note that Table III and Table IV focus on accuracy, model footprint, and robustness; for brevity, we do not explicitly tabulate the latency numbers here. Nevertheless, we also profiled the PyTorch-level wall-clock inference time of all three forecasters. The current Pro-LNN implementation adopts an unfused Python loop over time steps in eager mode, without any low-level kernel fusion or hand-optimized C++/CUDA operators. Thus, its measured per-inference latency is somewhat higher than that of the LSTM and Transformer baselines, even though it is much more compact in terms of parameter count and memory footprint. This gap should be viewed as an engineering artifact of the reference implementation rather than a structural limitation of the liquid architecture: with standard systems optimizations (e.g., kernel fusion and custom CUDA kernels on edge GPUs/NPUs), the runtime of Pro-LNN can be substantially reduced. Moreover, in Off-AIC<sup>2</sup>, the demand forecasting module is executed during the offline Stage, so a moderate prediction latency will not impact online ES–AgP trading and task scheduling.

### C. Performance Evaluation on Our FUSION

To emulate heterogeneous online demands across different ESs, we leverage the real-world UCI dataset [32], where each ES is associated with a distinct load profile. We train Pro-LNN on these profiles to forecast per-ES demand traces<sup>6</sup>, and then evaluate our framework under both synthetic ES-location settings (Sec. VI-C1–Sec. VI-C3) and real-world ES deployments derived from the EUA dataset [33] (Sec. VI-C4).

1) *Social Welfare*: SW represents one primary metric for evaluating the effectiveness of FUSION. Fig. 2(a)–2(b) report SW performance when the number of ESs increases from 8 to 16. The two subfigures correspond to two representative network configurations, i.e., 80 HuUs, 80 MaUs, and 5 AgPs in

<sup>6</sup>We employ the UCI dataset as a trace to learn realistic temporal patterns of aggregate demand at each ES. Pro-LNN is trained on these time series and used to forecast the ES  $s_i$ 's demand  $N_i^{\text{Dem},(t)}$  over future trading rounds; the forecasted demand profiles drive the time-varying HuU/MaU task arrival intensities at each ES, while the total population sizes of HuUs, MaUs, ESs, and AgPs are fixed to control the overall ecosystem scale.

Fig. 2(a), and 90 HuUs, 90 MaUs, and 7 AgPs in Fig. 2(b), so as to capture the overall trends under different market scales.

In Fig. 2(a), as the number of ESs grows from 8 to 16, SW of all methods increases, because involving more ESs introduces additional computing resources and service opportunities, thereby improving the overall utility. However, the growth rates differ significantly across different methods. FUSION consistently achieves the highest SW, and its advantage turns to be more pronounced when the number of ESs is larger (14 and 16). This is because, in the offline stage, FUSION employs Off-AIC<sup>2</sup> to orderly match AgP resources with ESs that have high potential revenue and favorable spatio-temporal locations, and in the online stage, it uses a PG-BRD based scheduler to perform congestion-aware task allocation among HuUs and MaUs. Thus, resources are exploited more sufficiently and fairly. PurOnline operates entirely without an offline stage and relies solely on an online potential game defined over the current topology. Lacking pre-planned routes to proactively reposition UAV resources, it achieves the lowest SW. FUSION\_NoPG shares the same offline stage as FUSION, but replaces PG-BRD with simple random assignment in the online stage. The resulting congestion cannot be effectively mitigated, leading to a clearly lower SW than FUSION, which indicates that the online potential game is crucial for realizing the full value of offline contracts. FUSION\_Random randomly associates AgPs with ESs in the offline stage, while still adopting PG-BRD in the online stage; its performance lies between FUSION and FUSION\_NoPG, implying that even with an intelligent online scheduler, the lack of revenue- and spatio-temporal-aware offline route planning still wastes a substantial amount of AgP capacity. FUSION\_NoST ignores ES spatio-temporal characteristics in the offline stage and only performs a simple price-driven auction, while keeping PG-BRD online. It outperforms PurOnline and FUSION\_Random, but still shows a stable gap to our FUSION, demonstrating that explicitly incorporating ES time windows and travel costs into offline contracts is a key to boosting SW.

Fig. 2(b) presents qualitatively similar results under the other network configuration. As the number of ESs grows, SW continues to rise over all methods, and our FUSION always ranks first. Comparing to Fig. 2(a), the overall welfare level is higher, and FUSION still achieves the best performance. Overall, these results show that, on the one hand, a well-designed offline AgP–ES contracting mechanism (especially Off-AIC<sup>2</sup> with explicit spatio-temporal and routing considerations) can continuously unlock potential gains as the system scales up; on the other hand, the PG-BRD based online scheduling stage effectively alleviates resource congestion on the SP side and further improves resource utilization. Working in tandem, these two stages enable FUSION to outperform representative baselines under various market scales.

2) *Evaluation on Interaction Overhead*: To quantitatively assess interaction efficiency, we consider two key metrics in DoI (Fig. 3(a)) and ECoI (Fig. 3(b)). The x-axis from s1 to s6 corresponds to different system configurations (i.e., different combinations of HuUs/MaUs/ESs/AgPs), and the y-axis is plotted on a logarithmic scale to better visualize the results across different magnitudes.

Overall, for all settings, the values of DoI and ECoI for different methods remain within the same order of magnitude, indicating that the interaction overhead is acceptable in all cases. Our FUSION is not strictly the best in terms of DoI

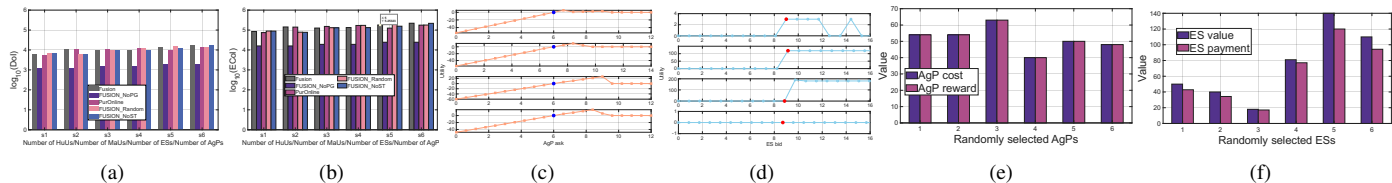


Fig. 3. Performance comparisons and property analyses, where (a)–(b) DoI and ECoI under different problem sizes (s1–s6 are set as {75/75/15/8}, {75/75/20/8}, {90/90/20/10}, {90/90/25/10}, {115/115/25/12}, and {115/115/30/12}), (c)–(d) truthfulness, and (e)–(f) individual rationality.

and ECoI, but the gaps between FUSION and the baselines (FUSION\_NoPG, FUSION\_Random, FUSION\_NoST, and PurOnline) are rather limited. This is due to the offline contracting stage in FUSION exposes more candidate SPs and richer resource options to the online scheduler. Accordingly, the PG-BRD based online stage calls for exploring a larger strategy space, which slightly increases the number of interaction rounds and signaling overhead per transaction.

It is worth emphasizing that both the auction and route planning in FUSION are executed in the offline stage, and thus do not introduce extra delay or energy consumption to the real-time online stage. The DoI and ECoI values reported in Fig. 3(a) and Fig. 3(b) already amortize this offline overhead in the overall assessment. When combined with SW in Fig. 2, we can observe that, while keeping DoI and ECoI at the same order of magnitude as the baselines and only incurring a modest increase, FUSION achieves a substantial improvement in SW by enabling more efficient exploitation of air–ground cooperative resources. In contrast, PurOnline may enjoy slightly lower DoI/ECoI in some, but its lack of offline pre-deployment and route planning leads to significantly worse SW. Similarly, FUSION\_NoPG, FUSION\_Random, and FUSION\_NoST exhibit interaction metrics comparable to FUSION, yet fail to reach the same utility level because they either remove PG-BRD or ignore ES spatio–temporal characteristics. In summary, FUSION maintains interaction overhead comparable to representative baselines, while simultaneously delivering much higher SW, thereby achieving a favorable trade-off between interaction cost and overall system benefit.

3) *Truthfulness and Individual Rationality*: Since truthfulness and individual rationality are two fundamental economic properties of auction mechanisms, we conduct a dedicated numerical study for the designed Off-AIC<sup>2</sup> offline auction embedded in FUSION. Unless otherwise specified, the simulations are performed under a representative setting with 75 HuUs, 75 MaUs, 12 ESs, and 7 AgPs. In particular, Fig. 3(c) and Fig. 3(d) illustrate how the utilities of buyers and sellers change with their reported bids/asks under this setting, while Fig. 3(e) and Fig. 3(f) verifies individual rationality from the perspectives of cost/value versus final payments.

Four subplots are presented in Fig. 3(c), each corresponding to an independent market instance. In every subplot, we randomly select one AgP as a representative. The horizontal axis denotes its reported ask, and the vertical axis shows the resulting utility obtained by this AgP in Off-AIC<sup>2</sup>. The red dot indicates its true ask, and the blue dot marks the critical transaction price obtained by the binary-search procedure, i.e., the largest ask at which the AgP still remains in the winning set when all other participants keep their bids/asks unchanged. We can observe that, as the ask increases from zero, the AgP’s utility grows approximately linearly and reaches a peak around the critical price, but drops to zero once the ask exceeds this threshold due to losing the contract. This behavior implies

that reporting an ask close to its true value yields (almost) the highest utility for the AgP, whereas over-reporting only increases the risk of being rejected without bringing additional gain, which numerically supports an “approximately truthful” property on the seller side.

Fig. 3(d) shows a symmetric analysis for ES as service buyers. In each subplot, one ES is randomly chosen, with the horizontal axis representing its reported mean bid (generated by scaling its true bid row) and the vertical axis depicting the utility defined as the true valuation minus the payment. Again, the red dot corresponds to the true bid and the blue dot to the critical bid returned by binary search. When the reported bid is lower than the critical value, the ES cannot win any contract and its utility stays at zero. Once the bid slightly exceeds the critical threshold, the ES becomes a winner and obtains a positive utility. Further increasing the bid does not change the matching result but only raises the payment, thereby shrinking the utility. Therefore, Fig. 3(d) indicates that bidding around the true valuation is also the best strategy for ESs, and misreporting does not significantly improve their utilities, which confirms truthfulness on the buyer side.

Fig. 3(e) and Fig. 3(f) then examines the individual rationality of Off-AIC<sup>2</sup>. In Fig. 3(e), several AgPs that successfully participate in the offline stage are randomly selected, and for each of them we compare its true total cost (unit cost times the actually served quantity) with the total reward determined by Off-AIC<sup>2</sup>. The bars clearly show that the “AgP reward” is never smaller than the corresponding “AgP cost” for any selected AgP, meaning that every winning seller can always cover its serving and traveling cost, hence satisfying seller-side individual rationality. Fig. 3(f) performs a similar comparison for randomly selected ESs, where each ES’s true valuation is compared against its final payment. The results demonstrate that “ES value” is always no less than “ES payment”, implying that no buyer suffers a loss in Off-AIC<sup>2</sup>, and thus buyer-side individual rationality is guaranteed. Overall, these results show that the Off-AIC<sup>2</sup> auction in the FUSION method can maintain approximate two-sided truthfulness and individual rationality under complex “vehicle-carried UAV with time-window and routing” constraints, while achieving high SW, making it a practical and robust solution for offline contract design in dynamic air–ground cooperative computing systems.

4) *Experiments on a Real-World Dataset*: To further evaluate the performance of all schemes under real-world deployments, we leverage the real-world EUA dataset [33]. Specifically, we

TABLE V  
PERFORMANCE COMPARISONS IN TERMS OF SW, DOI, AND ECOI  
(ALG. 1: FUSION, ALG. 2: FUSION\_NoPG, ALG. 3: PURONLINE, ALG. 4: FUSION\_RANDOM, ALG. 5: FUSION\_NoST)

Performance	Alg. 1	Alg. 2	Alg. 3	Alg. 4	Alg. 5
Social welfare	45104.55	40895.51	2771.04	3901.38	33229.09
DoI (s)	145.32	14.40	93.45	67.38	123.59
ECoI (W)	1865.80	191.50	1242.90	896.20	1643.80

extract a representative dense urban region from the Melbourne metropolitan area and construct a scenario with 125 ESs, 900 HuUs, 900 MaUs, and 80 AgPs according to the ES distributions provided in the dataset. Based on this setting, Table V reports the resulting SW, DoI, and ECoI. The results show that FUSION achieves a markedly higher SW than all baseline methods, with SW on the order of  $4.5 \times 10^4$ , significantly outperforming the pure online scheme PurOnline and the two-stage variants that lack spatio-temporal awareness or refined route planning. Meanwhile, the DoI and ECoI of FUSION remain comparable to those of other two-stage schemes, indicating that the offline Off-AIC<sup>2</sup> auction, although introducing additional contract and routing procedures in Stage I, does not cause unacceptable delay or energy overhead in the online phase. In contrast, FUSION\_NoPG attains the lowest interaction overhead but suffers from a substantial loss in SW due to the absence of potential-game-based scheduling in Stage II; FUSION\_Random and FUSION\_NoST demonstrate that ignoring the underlying payoff structure or ES spatio-temporal constraints in the offline phase leads to clearly inferior SW, even when the same PG-based online scheduler is employed. Overall, the results on the EUA dataset confirm that, in a large-scale real-world network, FUSION attains the best trade-off between utility and interaction cost by significantly improving SW while keeping interaction delay and energy consumption at a level comparable to other two-stage baselines.

## VII. CONCLUSION

In this work, we have proposed FUSION, a forecasting-driven, two-stage framework for sustainable service provisioning in air-ground integrated edge networks with human-machine coexistence. At the offline stage, we leveraged Pro-LNN to capture multi-step spatio-temporal dynamics of ES workloads, and integrated its predictions into eACOVRP and Off-AIC<sup>2</sup> to jointly plan AgP routes and design incentive-compatible ES-AgP contracts. At the online stage, we formulated congestion-aware task scheduling as an ordinal potential game over heterogeneous HuUs, MaUs, and ES/UAV providers, and developed the PG-BRD algorithm that converges to a pure-strategy NE while satisfying coverage and capacity constraints.

Simulation results on synthetic and real-world datasets demonstrate that FUSION consistently reduces latency, enhances SW, and improves resource utilization compared with purely online schemes, time-window-unaware routing, and greedy or random baselines, while empirically preserving individual rationality, budget balance, and near-truthfulness in Off-AIC<sup>2</sup>. These findings highlight the importance of tightly coupling prediction, routing, economic incentives, and game-theoretic scheduling under realistic spatio-temporal dynamics. Future work will incorporate more fine-grained model heterogeneity for AI inference/training services, and explore learning-enhanced or reinforcement-learning-based mechanisms that further adapt to long-term environmental and behavioral evolution.

## REFERENCES

- [1] L. Kong, J. Tan, J. Huang, G. Chen, S. Wang, X. Jin, P. Zeng, M. Khan, and S. K. Das, "Edge-computing-driven Internet of Things: A survey," *ACM Comput. Surv.*, vol. 55, no. 8, Art. no. 174, pp. 1-41, Dec. 2023.
- [2] Z. Ning, H. Hu, X. Wang, L. Guo, S. Guo, G. Wang, and X. Gao, "Mobile edge computing and machine learning in the Internet of unmanned aerial vehicles: A survey," *ACM Comput. Surv.*, vol. 56, no. 1, Art. no. 13, pp. 1-31, Aug. 2024.
- [3] H. Qi, M. Liwang, X. Wang, L. Li, W. Gong, J. Jin, and Z. Jiao, "Bridge the Present and Future: A Cross-Layer Matching Game in Dynamic Cloud-Aided Mobile Edge Networks," *IEEE Trans. Mobile Comput.*, vol. 23, no. 12, pp. 12522-12523, Dec. 2024.
- [4] G. Sun, Y. Wang, Z. Sun, Q. Wu, J. Kang, D. Niyato, and V. C. M. Leung, "Multi-objective optimization for multi-UAV-assisted mobile edge computing," *IEEE Trans. Mobile Comput.*, vol. 23, no. 12, pp. 14803-14820, 2024.
- [5] M. Hui, J. Chen, L. Yang, L. Lv, H. Jiang, and N. Al-Dhahir, "UAV-assisted mobile edge computing: Optimal design of UAV altitude and task offloading," *IEEE Trans. Wireless Commun.*, vol. 23, no. 10, pp. 13633-13647, Oct. 2024.
- [6] X. Wang, J. Li, J. Wu, L. Guo, and Z. Ning, "Energy efficiency optimization of IRS and UAV-assisted wireless powered edge networks," *IEEE J. Sel. Topics Signal Process.*, vol. 18, no. 7, pp. 1297-1310, 2024.
- [7] J. Xu, H. Yao, R. Zhang, T. Mai, and M. Guizani, "Low latency and accuracy-guaranteed DNN inference for UAV-assisted IoT networks," *IEEE Trans. Cogn. Commun. Netw.*, early access, 2025, doi: 10.1109/TCCN.2025.3542443.
- [8] Y. Li, J. Rao, L. Wang, Y. Xiao, X. Ge, and G. Shi, "Distributed optimization of resource efficiency for federated edge intelligence in AAV-enabled IoT networks," *IEEE Internet Things J.*, vol. 12, no. 8, pp. 9449-9464, Apr. 2025.
- [9] L. Zeng, H. Chen, D. Feng, X. Zhang, and X. Chen, "A3D: Adaptive, accurate, and autonomous navigation for edge-assisted drones," *IEEE/ACM Trans. Netw.*, vol. 32, no. 1, pp. 713-728, Feb. 2024.
- [10] S. Shen, K. Yang, K. Wang, and G. Zhang, "UAV-aided vehicular short-packet communication and edge computing system under time-varying channel," *IEEE Trans. Veh. Technol.*, vol. 72, no. 5, pp. 6625-6638, May 2023.
- [11] J. Tang, K. Fan, S. Yang, A. Liu, N. N. Xiong, H. H. Song, and V. C. M. Leung, "CPDZ: A credibility-aware and privacy-preserving data collection scheme with zero-trust in next-generation crowdsensing networks," *IEEE J. Sel. Areas Commun.*, vol. 43, no. 6, pp. 2183-2199, 2025.
- [12] Y. Ding, K. Li, C. Liu, and K. Li, "A Potential Game Theoretic Approach to Computation Offloading Strategy Optimization in End-Edge-Cloud Computing," *IEEE Trans. Parallel Distrib. Syst.*, vol. 33, no. 6, pp. 1503-1519, Jun. 2022.
- [13] Z. Zhou, L. Pan, and S. Liu, "Potential Game-Based Computation Offloading in Edge Computing With Heterogeneous Edge Servers," *IEEE Trans. Netw. Sci. Eng.*, vol. 12, no. 1, pp. 290-301, Jan. 2025.
- [14] C. Zhang, C. Lee, D. Niyato, and P. Wang, "Auction approaches for resource allocation in wireless systems: A survey," *IEEE Commun. Surveys Tuts.*, vol. 15, no. 3, pp. 1020-1041, 3rd Quart., 2013.
- [15] H. Ren, K. Liu, G. Yan, C. Liu, Y. Li, C. Li, and W. Wu, "Truthful auction mechanisms for dependent task offloading in vehicular edge computing," *IEEE Trans. Mobile Comput.*, vol. 23, no. 12, pp. 14987-15002, Dec. 2024.
- [16] X. Xu, Y. Hu, G. Cui, L. Qi, W. Dou, and Z. Cai, "CADEC: A combinatorial auction for dynamic distributed DNN inference scheduling in edge-cloud networks," *IEEE Trans. Mobile Comput.*, vol. 24, no. 10, pp. 10024-10041, Oct. 2025.
- [17] X. Li, K. Mo, Y. Hou, Z. Li, H. Xu, and N. Guan, "An online auction approach to computing resource allocation in mobile AIGC networks," *IEEE Internet Things J.*, vol. 12, no. 8, pp. 11182-11193, Apr. 2025.
- [18] R. Lu, W. Zhang, Y. Wang, Q. Li, X. Zhong, H. Yang, and D. Wang, "Auction-based cluster federated learning in mobile edge computing systems," *IEEE Trans. Parallel Distrib. Syst.*, vol. 34, no. 4, pp. 1145-1158, Apr. 2023.
- [19] C.-Y. Hsieh, Y. Ren, and J.-C. Chen, "Edge-cloud offloading: Knapsack potential game in 5G multi-access edge computing," *IEEE Trans. Wireless Commun.*, vol. 22, no. 11, pp. 7158-7171, Nov. 2023.
- [20] L. Wu, P. Sun, Z. Wang, Y. Li, and Y. Yang, "Computation offloading in multi-cell networks with collaborative edge-cloud computing: A game theoretic approach," *IEEE Trans. Mobile Comput.*, vol. 23, no. 3, pp. 2093-2106, Mar. 2024.
- [21] A. R. Hossain, W. Liu, and N. Ansari, "AI-native end-to-end network slicing for next-generation mission-critical services," *IEEE Trans. Cogn. Commun. Netw.*, vol. 11, no. 1, pp. 48-58, 2025.
- [22] S. Wu, M. Liwang, D. Wang, X. Wang, C. Wu, J. Tang, L. Li, and X. Xia, "Effective two-stage double auction for dynamic resource provision over edge networks via discovering the power of overbooking," *IEEE Trans. Serv. Comput.*, early access, pp. 1-13, 2025.
- [23] M. Chahine, R. Hasani, P. Kao, A. Ray, R. Shubert, M. Lechner, A. Amini, and D. Rus, "Robust flight navigation out of distribution with liquid neural networks," *Sci. Robot.*, vol. 8, no. 77, Art. eadc8892, 2023.
- [24] J. L. Ba, J. R. Kiros, and G. E. Hinton, "Layer normalization," arXiv preprint arXiv:1607.06450, 2016.

- [25] H. Qi, M. Liwang, X. Wang, L. Fu, Y. Hong, L. Li, and Z. Cheng, "Accelerating stable matching between workers and spatial-temporal tasks for dynamic MCS: A stagewise service trading approach," *IEEE Trans. Mobile Comput.*, early access, pp. 1-16, 2025, doi: 10.1109/TMC.2025.3610915.
- [26] J. Li, Y. Xiong, and J. She, "UAV path planning for target coverage task in dynamic environment," *IEEE Internet Things J.*, vol. 10, no. 20, pp. 17734-17745, 2023.
- [27] S. Hochreiter and J. Schmidhuber, "Long short-term memory," *Neural Comput.*, vol. 9, no. 8, pp. 1735-1780, Nov. 1997, doi: 10.1162/neco.1997.9.8.1735.
- [28] A. Vaswani, N. Shazeer, N. Parmar, J. Uszkoreit, L. Jones, A. N. Gomez, Ł. Kaiser, and I. Polosukhin, "Attention is all you need," in *Proc. Adv. Neural Inf. Process. Syst. (NeurIPS)*, 2017.
- [29] H. Qi, M. Liwang, S. Hosseinalipour, L. Fu, S. Zou, and W. Ni, "Future resource bank for ISAC: Achieving fast and stable win-win matching for both individuals and coalitions," *IEEE J. Sel. Areas Commun.*, early access, 2025, doi: 10.1109/JSAC.2025.3608114.
- [30] 5G Americas, "New services & applications with 5G ultra-reliable low latency communications," White Paper, Nov. 2018.
- [31] 3GPP, "5G; Study on scenarios and requirements for next generation access technologies," 3GPP TR 38.913, ver. 17.0.0, Release 17, 2022.
- [32] A. Trindade, "ElectricityLoadDiagrams20112014," UCI Mach. Learn. Repository, 2015. [Online]. Available: <https://doi.org/10.24432/C58C86>.
- [33] P. Lai, Q. He, M. Abdelrazek, F. Chen, J. Hosking, J. Grundy, and Y. Yang, "Optimal edge MU allocation in edge computing with variable sized vector bin packing," *Int. Conf. Service-Oriented Comput. (ICSOC)*, Springer, 2018, pp. 230-245.

APPENDIX A  
KEY NOTATIONS

Key notations in this paper are summarized in Table VI.

APPENDIX B  
DETAILED PRO-LNN ARCHITECTURE AND TRAINING  
PROCEDURE

In this section, we provide the detailed update equations and training procedure of the proposed Pro-LNN predictor used in Off-AIC<sup>2</sup>.

**Step 1. Stable liquid cell.** At the core of Pro-LNN is a stable liquid cell that updates a hidden state  $\mathbf{h}_i^{(\nu)} \in \mathbb{R}^d$  given the current input  $\mathbf{z}_i^{(\nu)}$  and the previous state. Concretely, we first compute neuron-wise time constants and a pre-activation:  $\tau^{(\nu)} = \text{softplus}(W_\tau[\mathbf{z}_i^{(\nu)}, \mathbf{h}_i^{(\nu)}]) + \tau_{\min}$  and  $\tilde{\mathbf{u}}^{(\nu)} = W_h \mathbf{h}_i^{(\nu)} + W_x \mathbf{z}_i^{(\nu)} + \mathbf{b}$ , where  $W_\tau, W_h, W_x$  and  $\mathbf{b}$  are trainable, and  $\tau_{\min} > 0$  enforces strictly positive time scales (we also clamp  $\tau^{(\nu)}$  to  $[\tau_{\min}, \tau_{\max}]$  for numerical stability). The effective update rate is then  $\alpha^{(\nu)} = \text{clip}\left(\frac{\Delta\nu}{\tau^{(\nu)}}, \alpha_{\min}, \alpha_{\max}\right)$ , with a fixed  $\Delta\nu$  (one trading interval in our implementation) and small constants  $0 < \alpha_{\min} \leq \alpha_{\max} < 1$ . We then apply a lightweight layer normalization and non-linearity,  $\tilde{\mathbf{h}}_i^{(\nu)} = \tanh(\text{LN}(\tilde{\mathbf{u}}^{(\nu)}))$ , and update the hidden state as

$$\mathbf{h}_i^{(\nu+1)} = (1 - \alpha^{(\nu)}) \odot \mathbf{h}_i^{(\nu)} + \alpha^{(\nu)} \odot \tilde{\mathbf{h}}_i^{(\nu)} + \gamma \tanh(\text{LN}(\mathbf{h}_i^{(\nu)})), \quad (24)$$

where  $\gamma$  is a small residual scaling factor and  $\odot$  denotes element-wise multiplication. This leaky-integrator update blends exponential memory decay with input-driven state injection, while the neuron-wise  $\tau^{(\nu)}$  allow different neurons to operate at different effective time scales.

*Notation.* For clarity, all nonlinear operators in the above update are applied element-wise unless otherwise stated. Specifically,  $\text{softplus}(\cdot)$  denotes the standard softplus activation  $\text{softplus}(x) = \log(1 + e^x)$ ,  $\text{clip}(x, a, b)$  clips each element of  $x$  into the interval  $[a, b]$ ,  $\text{LN}(\cdot)$  denotes layer normalization [24], and  $\text{LiquidCell}(\mathbf{z}_i^{(\nu)}, \mathbf{h}_i^{(\nu)})$  is a shorthand for one step of the stable liquid update in Step 1 (using the time-constant gating and residual integration described above).

**Step 2. Historical encoding.** Given the latest  $L$  observations of ES  $s_i$  up to trading round  $\nu$ , Pro-LNN encodes the history by iteratively applying the liquid cell:  $\mathbf{h}_i^{(\nu-L+1)} \leftarrow \text{LiquidCell}(\mathbf{z}_i^{(\nu-L+1)}, \mathbf{0}), \dots, \mathbf{h}_i^{(\nu)} \leftarrow \text{LiquidCell}(\mathbf{z}_i^{(\nu)}, \mathbf{h}_i^{(\nu-1)})$ .

This exponential-style integration naturally adapts memory decay and information injection under irregular or noisy trajectories.

**Step 3. Multi-horizon readout and consistency.** After encoding the history, a shallow MLP readout maps the final hidden state to an  $H$ -step forecast:

$$\hat{\mathbf{n}}_i^{(1:H)} = \text{Readout}(\mathbf{h}_i^{(\nu)}) = [\hat{N}_i^{\text{Dem},(\nu+1)}, \dots, \hat{N}_i^{\text{Dem},(\nu+H)}], \quad (25)$$

where  $\text{Readout}(\cdot)$  denotes a lightweight fully connected network that maps the  $d$ -dimensional hidden state to an  $H$ -dimensional prediction vector. The base training loss is the mean squared error (MSE) over the  $H$  horizons. To further improve stability for long horizons, we optionally add a *multi-step consistency* objective: starting from a history window, we repeatedly roll the model forward in closed loop by feeding its own one-step predictions back into the window, and penalize the mismatch at each rolled-out step.

**Step 4. Inference and integration.** At inference, Pro-LNN takes, for each ES  $s_i$ , the latest  $L$  observations

TABLE VI  
KEY NOTATIONS

Notation	Explanation
$\mathcal{S}, \mathcal{U}^H, \mathcal{U}^A, \mathcal{V}$	Sets of edge servers (ESs), human users (HuUs), machine users (MaUs), and air-ground providers (AgPs)
$s_i, u_m^H, u_n^A, v_k$	The $i$ -th ES, the $m$ -th HuU, the $n$ -th MaU, and the $k$ -th AgP
$N_i^{\text{Dem},(\nu)}, \hat{N}_i^{\text{Dem},(\nu+H)}$	Actual and LNN-predicted task demand of ES $s_i$ at trading rounds $\nu$ and $\nu+H$
$l_i^E, l_m^H, l_n^A, l_k^V$	3D locations of ES $s_i$ , HuU $u_m^H$ , MaU $u_n^A$ , and the dispatching vehicle of AgP $v_k$
$r_m^H, r_n^A, r_j$	Computation workload (CPU cycles) of HuU $u_m^H$ , MaU $u_n^A$ , and generic SD $u_j^{\text{On}}$
$d_m^H, d_n^A, d_j$	Input data size (bits) of HuU tasks, MaU tasks, and generic SD tasks
$f_i^E, f_i^{\text{On}}, f_m^{\text{H,loc}}, f_n^{\text{A,loc}}, f_k^{\text{V}}$	Computing capabilities of ES $s_i$ , online SP $s_i^{\text{On}}$ , local HuU/MaU devices, and UAVs dispatched by AgP $v_k$
$e_m^{\text{H,tx}}, e_n^{\text{A,tx}}$	Uplink transmit power of HuU $u_m^H$ and MaU $u_n^A$
$e_i^E$	Local computing energy consumption of ES $s_i$
$e_k^{\text{comp}}, e_k^{\text{move}}, e_k^{\text{fly}}$	Energy consumption of AgP $v_k$ for computation, ground movement, and UAV flight
$\tau_n^{\text{ddl}}, D_j$	Task deadline of MaU $u_n^A$ in Stage I and latency deadline of SD $u_j^{\text{On}}$ in Stage II
$C_k^V$	Total number of UAVs carried by AgP $v_k$
$N_{i,k}^{\text{Trad}}$	Quantity of traded computing resources between ES $s_i$ and AgP $v_k$ in an offline contract
$x_{i,k}^{\text{Off}}, \mathbf{X}$	Binary offline assignment between ES $s_i$ and AgP $v_k$ ; $\mathbf{X}$ collects all $x_{i,k}^{\text{Off}}$
$p_{i,k}^{\text{ES}}, r_{i,k}^{\text{ES}}, \tilde{p}_i$	Payment from ES $s_i$ to AgP $v_k$ , reward received by $v_k$ , and historical average user service price at $s_i$
$U^{\text{ES,Off}}, U_k^V, U^{\text{Auc}}$	Utility of ES $s_i$ , utility of AgP $v_k$ , and utility of the auctioneer in Stage I
$U^{\text{SW}}$	Total SW of the offline auction market (sum of utilities of ESSs, AgPs, and auctioneer)
$\mathcal{G}_k(\mathcal{N}_k, \mathcal{E}_k), \mathbb{K}$	Directed complete graph and ant set used by eACO-VRP for routing AgP $v_k$
$\varphi_{r,s}, \eta_{r,s}, P_{n_r \rightarrow n_s}^k$	Pheromone level, distance, and transition probability on edge $(n_r, n_s)$ in eACO-VRP
$\mathcal{S}^{\text{On}}, \mathcal{U}^{\text{On}}, \mathcal{H}, \mathcal{A}$	Sets of online service providers (SPs), service demanders (SDs), HuUs and MaUs in Stage II
$x_i^{\text{On}}, x_{i,i}^{\text{On}}, x_j$	Indicator of local execution, indicator of scheduling SD $u_j^{\text{On}}$ to SP $s_i^{\text{On}}$ , and the scheduling vector of SD $u_j^{\text{On}}$
$y_i, x_i, n_i(\boldsymbol{\pi})$	Effective congestion load, aggregate computing load, and number of associated SDs at SP $s_i^{\text{On}}$ under profile $\boldsymbol{\pi}$
$t_{i,i}^{\text{comp}}, t_{i,i}^{\text{tx}}, T_{i,i}^{\text{edge}}$	Computation delay, uplink transmission delay, and total edge-side latency of SD $u_i^{\text{On}}$ at SP $s_i^{\text{On}}$
$S_j(\hat{u}), \kappa_j, \theta_{j,i}, \tau_i(y)$	Non-congestion benefit term, congestion sensitivity, load factor, and congestion function at SP $s_i^{\text{On}}$
$K_i(x_i), C_i$	Computation/operation cost function and maximum computing capacity of SP $s_i^{\text{On}}$
$\boldsymbol{\pi}, \Phi(\boldsymbol{\pi}), \mathcal{F}^I, \mathcal{F}^{II}$	Joint scheduling profile, ordinal potential function, and optimization problems in Stage I and Stage II

**Algorithm 4: Pro-LNN**


---

**Input:** Training sequences  $\{z_i^{(1:T)}\}$ ; history length  $L$ ; horizon  $H$ ; learning rate  $\eta$ ; consistency depth  $K$

**Output:** Predicted sequences  $\{\hat{N}_i^{\text{Dem},(\nu+1:\nu+H)}\}$

- 1 Initialize liquid-cell and readout parameters  $\theta$ ;
- 2 **while** *not converged* **do**
- 3     Sample a mini-batch  $\mathcal{B}$  of training windows from  $\mathcal{D}$ ;
- 4     **for** each window  $(z_i^{(\nu-L+1:\nu)}, N_i^{\text{Dem},(\nu+1:\nu+H)}) \in \mathcal{B}$  **do**
- 5         Set hidden state  $\mathbf{h}_i \leftarrow \mathbf{0}$ ;
- 6         **for**  $k = \nu - L + 1$  **to**  $\nu$  **do**
- 7              $\mathbf{h}_i \leftarrow \text{LiquidCell}(z_i^{(k)}, \mathbf{h}_i)$ ;
- 8         **(Base  $H$ -step forecast)**
- 9          $\hat{\mathbf{n}}_i^{(1:H)} \leftarrow \text{Readout}(\mathbf{h}_i)$ ;
- 10          $\mathcal{L}_i \leftarrow \frac{1}{H} \sum_{h=1}^H (\hat{n}_i^{(h)} - N_i^{\text{Dem},(\nu+h)})^2$ ;
- 11         **if**  $K > 0$  **then**
- 12             Construct a history window  $\mathbf{y}_i$  from  $\{z_i^{(\nu-L+1)}, \dots, z_i^{(\nu)}\}$ ;
- 13             **for**  $k = 1$  **to**  $K$  **do**
- 14                  $\hat{\mathbf{n}}_i^{(1:H)} \leftarrow f_\theta(\mathbf{y}_i)$ ;
- 15                  $\mathcal{L}_i \leftarrow \mathcal{L}_i + (\hat{n}_i^{(1)} - N_i^{\text{Dem},(\nu+k)})^2$ ;
- 16                 Update  $\mathbf{y}_i$  by discarding the oldest step and appending  $\hat{n}_i^{(1)}$  as the newest demand;
- 17              $\mathcal{L}_i \leftarrow \mathcal{L}_i / (H + K)$ ;
- 18     Aggregate loss  $\mathcal{L} \leftarrow \frac{1}{|\mathcal{B}|} \sum_{i \in \mathcal{B}} \mathcal{L}_i + \lambda \Omega(\theta)$ ;
- 19     Update parameters  $\theta \leftarrow \theta - \eta \nabla_\theta \mathcal{L}$ ;

---

$\{z_i^{(\nu-L+1)}, \dots, z_i^{(\nu)}\}$ , encodes them via the liquid cell into  $\mathbf{h}_i^{(\nu)}$ , and applies the readout to obtain an  $H$ -step forecast  $\{\hat{N}_i^{\text{Dem},(\nu+1)}, \dots, \hat{N}_i^{\text{Dem},(\nu+H)}\}$ . These predictions are computed in the offline stage before each trading round and then fed into: (i) the eACO-VRP module for time-window-aware ES recommendation and AgP route pre-planning, and (ii) the auction module for ES-AgP contract design. Since Pro-LNN runs offline, its wall-clock inference latency does not affect the real-time trading between SDs and SPs, while its compact footprint and robustness to noisy inputs make it well suited for deployment on edge and near-edge computing platforms.

## APPENDIX C

PROOF OF PROPERTY OF OFF-AIC<sup>2</sup>

**Theorem 2.** *All winning ESs and AgPs obtained from Off-AIC<sup>2</sup> are individually rational during the offline stage.*

*Proof.* The individual rationality of Off-AIC<sup>2</sup> is guaranteed by the core design of its allocation (Phase 2) and pricing (Phase 3) procedures in Alg. 2, under the single-parameter assumption that each ES  $s_i$  has a per-unit valuation and each AgP  $v_k$  has a per-unit cost.

(i) **ES side (buyers).** We first consider ES buyers  $s_i$ .

• *Allocation in Phase 2:* For each AgP  $v_k$ , the candidate ES set is constructed as

$$C_k = \{i \in \mathcal{U}^{\text{free}} \mid U_{i,k} > 0 \wedge \text{bid}_{i,k} \geq \overline{\text{bid}}_i\}, \quad (26)$$

where  $U_{i,k} = \text{bid}_{i,k} - \text{ask}_k$  denotes the surplus of matching ES  $s_i$  with AgP  $v_k$ . Hence, if ES  $s_i$  is eventually matched (i.e., there exists some  $k$  such that  $x_{i,k}^{\text{Off}} = 1$ ), the corresponding pair  $(i, k)$  must satisfy

$$U_{i,k} = \text{bid}_{i,k} - \text{ask}_k > 0, \quad \text{bid}_{i,k} \geq \overline{\text{bid}}_i. \quad (27)$$

Under truthful bidding,  $\text{bid}_{i,k}$  equals  $s_i$ 's true per-unit valuation for the contracted service. Therefore, already at the *allocation*

stage, every winning ES enjoys a strictly positive surplus margin between its valuation and the AgP's ask.

• *Pricing in Phase 3:* In Phase 3, for each winning ES  $s_i$  with  $\sum_k x_{i,k}^{\text{Off}} = 1$ , Off-AIC<sup>2</sup> treats its effective bid as a variable and performs a monotone binary search over an interval of the form

$$p_i^{\text{b*}} \in [\underline{b}_i, \overline{\text{bid}}_i], \quad (28)$$

where  $\overline{\text{bid}}_i$  is  $s_i$ 's reference bid (coinciding with its true valuation when truthful) and  $\underline{b}_i$  is a market-wide lower bound. The binary search stops at the *minimal* critical payment that keeps  $s_i$  in the winning set when Phase 2 is re-executed. By construction, we have

$$p_i^{\text{b*}} \leq \overline{\text{bid}}_i. \quad (29)$$

Moreover, for the realized winning pair  $(i, k)$  we also have  $\text{bid}_{i,k} \geq \overline{\text{bid}}_i$ . Combining these relations yields

$$\text{bid}_{i,k} \geq \overline{\text{bid}}_i \geq p_i^{\text{b*}}. \quad (30)$$

Under truthful bidding,  $\text{bid}_{i,k}$  is ES  $s_i$ 's true valuation, while  $p_i^{\text{b*}}$  is its actual per-unit payment in Off-AIC<sup>2</sup>. Hence the ex-post utility of  $s_i$  in the offline stage satisfies

$$u_i^{\text{ES}} = (\text{valuation}) - (\text{payment}) \geq \text{bid}_{i,k} - p_i^{\text{b*}} \geq 0, \quad (31)$$

which proves individual rationality for all winning ESs.

(ii) **AgP side (sellers).** We now turn to AgP sellers  $v_k$ .

• *Allocation in Phase 2:* In Phase 2, AgPs only serve ESs that yield strictly positive surplus, and they are protected by capacity constraints. Specifically,  $v_k$  may serve ES  $s_i$  only if  $U_{i,k} = \text{bid}_{i,k} - \text{ask}_k > 0$ , and the matching obeys

$$\sum_i x_{i,k}^{\text{Off}} N_i^{\text{Dem}} \leq C_k^{\text{V}}. \quad (32)$$

Under truthful reporting,  $\text{ask}_k$  equals  $v_k$ 's true per-unit cost. Thus each winning AgP only accepts contracts where the buyer-side valuation exceeds its cost, ensuring a nonnegative surplus margin at the allocation stage.

• *Pricing in Phase 3:* In Phase 3, for each winning AgP  $v_k$  with  $\sum_i x_{i,k}^{\text{Off}} \geq 1$ , Off-AIC<sup>2</sup> performs a monotone binary search over an interval

$$r_k^{\text{s*}} \in [\text{ask}_k, \bar{r}_k], \quad (33)$$

where  $\text{ask}_k$  is its own ask (true cost when truthful) and  $\bar{r}_k$  is a market-determined upper bound. The search stops at the *maximal* critical reward that still keeps  $v_k$  in the winning set when Phase 2 is rerun. Consequently,

$$r_k^{\text{s*}} \geq \text{ask}_k. \quad (34)$$

Under truthful reporting,  $\text{ask}_k$  is  $v_k$ 's true per-unit cost, and  $r_k^{\text{s*}}$  is the actual per-unit reward it receives. Hence the ex-post utility of  $v_k$  in the offline stage is

$$u_k^{\text{AgP}} = (r_k^{\text{s*}} - \text{ask}_k) \cdot \left( \sum_i x_{i,k}^{\text{Off}} N_i^{\text{Dem}} \right) \geq 0. \quad (35)$$

In summary, by construction of the candidate sets and critical-value pricing, every winning ES pays no more than its valuation, and every winning AgP receives no less than its cost. Therefore, Off-AIC<sup>2</sup> is individually rational for both ESs and AgPs in the offline stage. ■

**Theorem 3.** *Under the single-parameter assumption, the proposed Off-AIC<sup>2</sup> mechanism is truthful (dominant-strategy incentive-compatible) for both ESs and AgPs in the offline stage.*

*Proof.* The truthfulness of Off-AIC<sup>2</sup> follows from the fact that, on both the ES side and the AgP side, it implements a *monotone* allocation rule together with *critical-value* payments, which is sufficient for dominant-strategy incentive compatibility in single-parameter environments.

(i) **ES side (buyers).** Fix any ES  $s_i$  and treat all other bids and asks as given. Under the single-parameter assumption,  $s_i$  submits a single per-unit bid  $b_i$ , which induces its bid entries  $\text{bid}_{i,k} = b_i$  and average bid  $\overline{\text{bid}}_i = b_i$ .

- *Monotone allocation (Phases 1 & 2).* In Phase 1, ESs are sorted in nonincreasing order of  $\overline{\text{bid}}_i = b_i$ . Increasing  $b_i$  can only move  $s_i$  upward in this list; it can never push  $s_i$  to a worse rank. Since Off-AIC<sup>2</sup> only considers the top- $I^*$  ESs, once  $s_i$  belongs to the top- $I^*$  at some bid  $b_i$ , it remains in the top- $I^*$  for any higher bid  $b'_i > b_i$ .

In Phase 2, a necessary condition for  $s_i$  to be matched is that it lies in the top- $I^*$  ESs and that there exists an AgP  $v_k$  such that

$$U_{i,k} = \text{bid}_{i,k} - \text{ask}_k = b_i - \text{ask}_k > 0, \quad \text{bid}_{i,k} \geq \overline{\text{bid}}_i. \quad (36)$$

If  $s_i$  is selected at some bid  $b_i$ , then increasing its bid to  $b'_i > b_i$  strictly increases  $U_{i,k}$  for all  $k$  and does not violate any of the above inequalities. Under a fixed tie-breaking rule in the eACO-VRP procedure, any ES that is winning at  $b_i$  remains winning at any higher bid  $b'_i > b_i$ . Thus the ES-side allocation rule is monotone in  $b_i$ .

- *Critical payment (Phase 3).* In Phase 3, for each winning ES  $s_i$  (with  $\sum_k x_{i,k}^{\text{Off}} = 1$ ), Off-AIC<sup>2</sup> treats its effective bid as a variable and performs a monotone binary search over an interval

$$b_i^{\text{eff}} \in [b_i, \overline{\text{bid}}_i], \quad (37)$$

repeatedly re-running Phase 2 to check whether  $s_i$  would still be selected. The search stops at the *smallest* bid at which  $s_i$  remains a winner, and the resulting value is taken as its payment:

$$p_i^{\text{b*}} = \text{critical bid of } s_i. \quad (38)$$

By construction, this critical payment depends only on other participants' bids and asks and on the system parameters; it does not depend on the actual report  $b_i$  as long as  $b_i \geq p_i^{\text{b*}}$ . Consequently,  $s_i$  cannot reduce its payment by overbidding, and any underbid  $b_i < p_i^{\text{b*}}$  either keeps the allocation and payment unchanged (if  $s_i$  still wins) or makes it lose a profitable contract. Hence truthful bidding maximizes  $s_i$ 's utility, and Off-AIC<sup>2</sup> is truthful for ESs.

(ii) **AgP side (sellers).** We now fix an AgP  $v_k$  and consider its per-unit ask  $a_k$ , treating all ES bids and other AgPs' asks as fixed. Under the single-parameter assumption,  $a_k$  is  $v_k$ 's single strategic parameter.

- *Monotone allocation (Phases 1 & 2).* In Phase 1, AgPs are sorted in nondecreasing order of  $\text{ask}_k = a_k$ . Lowering  $a_k$  can only move  $v_k$  upward in this list, never downward. Since Off-AIC<sup>2</sup> only considers the top- $K^*$  AgPs, once  $v_k$  is in the top- $K^*$  at some ask  $a_k$ , it remains in the top- $K^*$  for any lower ask  $a'_k < a_k$ .

In Phase 2,  $v_k$ 's attractiveness to ESs is determined by the surplus terms

$$U_{i,k} = \text{bid}_{i,k} - a_k. \quad (39)$$

If  $v_k$  is selected at some ask  $a_k$ , then lowering its ask to  $a'_k < a_k$  strictly increases all  $U_{i,k}$ , making  $v_k$  (weakly) more competitive. Under the same capacity constraint and tie-breaking rule in eACO-VRP, this can never cause  $v_k$  to lose its winning status. Thus, once  $v_k$  is a winner at  $a_k$ , it remains a winner at any lower ask  $a'_k < a_k$ , so the seller-side allocation rule is monotone in  $-a_k$ .

- *Critical reward (Phase 3).* In Phase 3, for each winning AgP  $v_k$  (with  $\sum_i x_{i,k}^{\text{Off}} \geq 1$ ), Off-AIC<sup>2</sup> treats its effective ask as a variable and runs a monotone binary search over an interval

$$a_k^{\text{eff}} \in [\text{ask}_k, \bar{r}_k], \quad (40)$$

replaying Phase 2 to check whether  $v_k$  would still be selected. The search terminates at the *largest* ask at which  $v_k$  remains a winner, and the corresponding per-unit reward is set to

$$r_k^{\text{s*}} = \text{critical ask of } v_k. \quad (41)$$

This critical reward is fully determined by others' reports and system parameters; it does not depend on the actual ask  $a_k$  as long as  $a_k \leq r_k^{\text{s*}}$ . Therefore, increasing  $a_k$  above  $r_k^{\text{s*}}$  either has no effect (if  $v_k$  is still losing) or causes it to lose a profitable contract, while decreasing  $a_k$  below  $r_k^{\text{s*}}$  does not increase the reward it receives. As a result, truthful asking maximizes  $v_k$ 's utility, and Off-AIC<sup>2</sup> is truthful for AgPs.

Combining the ES-side and AgP-side arguments, we conclude that Off-AIC<sup>2</sup> implements a monotone allocation rule with critical-value payments for both buyers and sellers in a single-parameter setting. Hence the mechanism is truthful (dominant-strategy incentive-compatible) for both ESs and AgPs in the offline stage. ■

**Theorem 4.** *Off-AIC<sup>2</sup> satisfies the (weak) budget-balance property in the offline stage.*

*Proof.* To verify budget balance, it suffices to show that the auctioneer's utility in the offline stage,

$$U^{\text{P}} = \sum_{s_i \in \mathcal{S}} \sum_{v_k \in \mathcal{V}} x_{i,k}^{\text{Off}} N_{i,k}^{\text{Trad}} (p_{i,k}^{\text{ES}} - r_{i,k}^{\text{ES}}), \quad (42)$$

is nonnegative, i.e.,  $U^{\text{P}} \geq 0$ . Since  $N_{i,k}^{\text{Trad}} \geq 0$  and  $x_{i,k}^{\text{Off}} \in \{0, 1\}$ , this reduces to proving that for every active trading pair  $(i, k)$  with  $x_{i,k}^{\text{Off}} = 1$ ,

$$p_{i,k}^{\text{ES}} - r_{i,k}^{\text{ES}} \geq 0. \quad (43)$$

(i) **Phase 1 (pivotal-rank selection).** In Phase 1 of Alg. 2, ESs are sorted in nonincreasing order of their average bids  $\overline{\text{bid}}_i$ , and AgPs are sorted in nondecreasing order of their asks  $\text{ask}_k$ . The pivotal ranks  $(I^*, K^*)$  are chosen such that

$$\overline{\text{bid}}_{I^*} \geq \text{ask}_{K^*}, \quad \sum_{k=1}^{K^*} C_k^{\text{V}} \geq \sum_{i=1}^{I^*} N_i^{\text{Dem}}. \quad (44)$$

Alg. 2 only considers the top- $I^*$  ESs and top- $K^*$  AgPs for matching. Hence, for any winning pair  $(i, k)$  with  $x_{i,k}^{\text{Off}} = 1$ , we have

$$\text{bid}_{i,k} \geq \overline{\text{bid}}_{I^*} \geq \text{ask}_{K^*} \geq \text{ask}_k. \quad (45)$$

Equation (45) shows that, for each matched pair  $(i, k)$ , there exists a nonempty price band

$$\{(p, r) \mid \text{ask}_k \leq r \leq p \leq \text{bid}_{i,k}\} \quad (46)$$

in which both ES  $s_i$  and AgP  $v_k$  obtain nonnegative utilities and the auctioneer's per-unit margin  $p - r$  is nonnegative.

**(ii) Phase 3 (critical pricing).** Phase 3 of Alg. 2 determines the actual payments within this feasible band using critical-value binary searches:

- *Buyer side (ESs):* For each winning ES  $s_i$  with  $\sum_k x_{i,k}^{\text{Off}} = 1$ , the payment  $p_i^{\text{b*}}$  is obtained via a monotone binary search on its effective bid parameter. The search interval is chosen inside the buyer side of the surplus-feasible band in (45), and the algorithm stops at the minimum critical bid that keeps  $s_i$  in the winning set when Phase 2 is re-executed. Thus, for any matched pair  $(i, k)$ ,

$$p_{i,k}^{\text{ES}} = p_i^{\text{b*}} \leq \text{bid}_{i,k}. \quad (47)$$

- *Seller side (AgPs):* Similarly, for each winning AgP  $v_k$  with  $\sum_i x_{i,k}^{\text{Off}} \geq 1$ , the reward  $r_k^{\text{s*}}$  is obtained via a monotone binary search on its effective ask parameter. The search interval is chosen inside the seller side of the band in (45), and the algorithm stops at the maximum critical ask that keeps  $v_k$  in the winning set. Hence, for any matched pair  $(i, k)$ ,

$$r_{i,k}^{\text{ES}} = r_k^{\text{s*}} \geq \text{ask}_k. \quad (48)$$

Because both searches are confined to the common surplus-feasible band identified in (45), off-AIC<sup>2</sup> always chooses prices satisfying

$$\text{ask}_k \leq r_{i,k}^{\text{ES}} \leq p_{i,k}^{\text{ES}} \leq \text{bid}_{i,k}, \quad \forall (i, k) \text{ with } x_{i,k}^{\text{Off}} = 1. \quad (49)$$

In particular, we obtain

$$p_{i,k}^{\text{ES}} - r_{i,k}^{\text{ES}} \geq 0 \quad \forall (i, k) \text{ with } x_{i,k}^{\text{Off}} = 1. \quad (50)$$

**(iii) Concluding budget balance.** Therefore, each active trading pair contributes a nonnegative margin

$$x_{i,k}^{\text{Off}} N_{i,k}^{\text{Trad}} (p_{i,k}^{\text{ES}} - r_{i,k}^{\text{ES}}) \geq 0, \quad (51)$$

while unmatched pairs contribute zero. Summing over all ES–AgP pairs gives

$$U^{\text{P}} = \sum_{i,k} x_{i,k}^{\text{Off}} N_{i,k}^{\text{Trad}} (p_{i,k}^{\text{ES}} - r_{i,k}^{\text{ES}}) \geq 0, \quad (52)$$

which completes the proof that Off-AIC<sup>2</sup> is (weakly) budget balanced in the offline stage. ■

## APPENDIX D

### PROOF DETAILS FOR THE ORDINAL POTENTIAL AND PG-BRD

This appendix collects the main technical ingredients behind the ordinal-potential formulation in Stage II and the design of PG-BRD. We: (i) rewrite the model using a global assignment matrix, (ii) relate pointwise congestion penalties to integrated congestion via a simple sandwich inequality, (iii) characterize single-user deviations and the linearized soft-deadline utility, (iv) prove the ordinal-potential property and finite-improvement path (FIP), and (v) clarify why monetary payments are excluded from the potential.

### A. Matrix Formulation Based on the Global Assignment Matrix

For some of the theoretical arguments and for vectorized implementations, it is convenient to represent the joint offloading profile by a single global matrix.

**Global assignment matrix.** Define

$$\mathbf{X} \in \{0, 1\}^{|\mathcal{U}^{\text{On}}| \times (1 + |\mathcal{S}^{\text{On}}|)} \quad (53)$$

by stacking each SD's binary decision vector  $\mathbf{X}_j^{\text{On}} = (x_{j,0}^{\text{On}}, x_{j,1}^{\text{On}}, \dots, x_{j,|\mathcal{S}^{\text{On}}|}^{\text{On}})$ . The  $(j, 0)$ -th entry corresponds to local execution ( $\pi_j = 0$ ), and the  $(j, i)$ -th entry corresponds to offloading to  $s_i^{\text{On}}$  ( $\pi_j = i$ ). Under the one-hot per-row constraint  $\sum_i x_{j,i}^{\text{On}} + x_{j,0}^{\text{On}} = 1$ ,  $\mathbf{X}$  and  $\boldsymbol{\pi}$  are equivalent representations.

**Aggregates in matrix form.** Using  $\mathbf{X}$ , the effective congestion load and physical workload at SP  $s_i^{\text{On}}$  are

$$y_i(\mathbf{X}) = \sum_{j \in \mathcal{U}^{\text{On}}} \gamma_{j,i} x_{j,i}^{\text{On}}, \quad \mathbb{x}_i(\mathbf{X}) = \sum_{j \in \mathcal{U}^{\text{On}}} r_j x_{j,i}^{\text{On}}. \quad (54)$$

These expressions are directly usable in optimization-based or vectorized implementations of PG-BRD.

**Potential in matrix form.** Substituting (54) into the potential in (21), we obtain the equivalent representation

$$\begin{aligned} \Phi(\mathbf{X}) = & \sum_{j \in \mathcal{U}^{\text{On}}} \sum_{i \in \mathcal{S}^{\text{On}}} S_j(i) x_{j,i}^{\text{On}} - \sum_{i \in \mathcal{S}^{\text{On}}} \int_0^{y_i(\mathbf{X})} \tau_i(z) dz \\ & - \sum_{i \in \mathcal{S}^{\text{On}}} K_i(\mathbb{x}_i(\mathbf{X})), \end{aligned} \quad (55)$$

which coincides with  $\Phi(\boldsymbol{\pi})$  whenever each row of  $\mathbf{X}$  has exactly one nonzero entry. In this form,  $\Phi(\mathbf{X})$  decomposes into: (i) a linear term in non-congestion benefits, (ii) an integral term in congestion loads, and (iii) a convex term in SP costs.

### B. Integral–Pointwise Sandwich Inequality

To relate user-level congestion penalties to the integrated congestion term in the potential, we use a simple “sandwich” inequality for increasing functions.

**Lemma 1** (Integral–pointwise sandwich). *Let  $\tau_i : [0, \infty) \rightarrow [0, \infty)$  be nonnegative and increasing. For any  $y \geq 0$  and any  $\gamma_{j,i} > 0$ ,*

$$\gamma_{j,i} \tau_i(y_i) \leq \int_{y_i}^{y_i + \gamma_{j,i}} \tau_i(z) dz \leq \gamma_{j,i} \tau_i(y_i + \gamma_{j,i}). \quad (56)$$

*Sketch.* For all  $z \in [y_i, y_i + \gamma_{j,i}]$ , monotonicity gives  $\tau_i(y_i) \leq \tau_i(z) \leq \tau_i(y_i + \gamma_{j,i})$ . Integrating over this interval yields (56). Equivalently, by the mean-value theorem for integrals, the integral equals  $\gamma_{j,i} \tau_i(\xi)$  for some  $\xi \in [y_i, y_i + \gamma_{j,i}]$ , which directly implies the bounds. ■

**Interpretation.** The integral in (56) can be viewed as the average of pointwise congestion penalties between  $y_i$  and  $y_i + \gamma_{j,i}$ . Its sign changes exactly when the pointwise terms do, which is the key to aligning changes in the potential with changes in individual utilities.

For the linear-response model  $\tau_i(y) = y/f_i^{\text{On}}$ ,

$$\int_y^{y+\gamma} \tau_i(z) dz = \frac{(y+\gamma)^2 - y^2}{2f_i^{\text{On}}} = \frac{y\gamma}{f_i^{\text{On}}} + \frac{\gamma^2}{2f_i^{\text{On}}}, \quad (57)$$

so the integrated congestion level is  $(y + \frac{\gamma}{2})/f_i^{\text{On}}$ , which lies between  $\tau_i(y)$  and  $\tau_i(y + \gamma)$ .

### C. Single-User Deviation: Utility and Potential Changes

We next spell out the single-user deviation that underlies the ordinal-potential proof. The goal is to compare the sign of the utility change with that of the potential change.

**Deviation setup.** Fix an action profile  $\pi$  and SD  $u_j^{\text{On}}$ . Consider a unilateral deviation

$$\pi_j = \dot{i} \longrightarrow \pi'_j = \dot{i}', \quad \pi' = (\pi_{-j}, \dot{i}'). \quad (58)$$

By (20), the congestion loads at the two involved SPs satisfy

$$y_{i'}(\pi') = y_{i'}(\pi) + \gamma_{j,i'}, \quad (59)$$

$$y_i(\pi') = y_i(\pi) - \gamma_{j,i}. \quad (60)$$

The corresponding physical workloads evolve as

$$x_{i'}(\pi') = x_{i'}(\pi) + r_j, \quad x_i(\pi') = x_i(\pi) - r_j. \quad (61)$$

**Utility change.** Using the unified utility (19), the change in SD  $u_j^{\text{On}}$ 's utility is

$$\begin{aligned} \Delta U_j &= U_{j,i'} - U_{j,i} \\ &= \left( S_j(\dot{i}') - S_j(\dot{i}) \right) - \kappa_j \theta_{j,i'} \tau_i(y_{i'}(\pi')) + \kappa_j \theta_{j,i} \tau_i(y_i(\pi)) \\ &\quad - (p_{j,i'} - p_{j,i}). \end{aligned} \quad (62)$$

The first term is the change in non-congestion benefit, the next two terms capture the congestion effect, and the last term is a pure payment transfer.

**Potential change.** By (21), the potential change is

$$\begin{aligned} \Delta \Phi &= \Phi(\pi') - \Phi(\pi) \\ &= \underbrace{S_j(\dot{i}') - S_j(\dot{i})}_{\text{non-congestion benefit}} \\ &\quad - \underbrace{\left( \int_{y_{i'}(\pi)}^{y_{i'}(\pi) + \gamma_{j,i'}} \tau_i(z) dz - \int_{y_i(\pi) - \gamma_{j,i}}^{y_i(\pi)} \tau_i(z) dz \right)}_{\text{integrated congestion variation}} \\ &\quad - \underbrace{\left( K_{i'}(x_{i'}(\pi) + r_j) - K_{i'}(x_{i'}(\pi)) \right)}_{\text{SP } i' \text{ cost increase}} \\ &\quad + \underbrace{\left( K_i(x_i(\pi)) - K_i(x_i(\pi) - r_j) \right)}_{\text{SP } s_i^{\text{On}} \text{ cost decrease}}. \end{aligned} \quad (63)$$

Payment terms are absent from  $\Delta \Phi$  by construction (see Appx. D-I).

### D. Approximate Linearization of Soft-Deadline Utility

We briefly justify the linearized MaU utility in (18) and the definition of the congestion-sensitivity coefficient  $\kappa_j$ .

Recall that for MaU  $u_j^{\text{On}}$  offloading to  $s_i^{\text{On}}$ ,

$$G_{j,i}^A = v_j \frac{[D_j - T_{j,i}^{\text{edge}}]_+}{D_j}, \quad T_{j,i}^{\text{edge}} = t_{j,i}^{\text{comp}} + t_{j,i}^{\text{tx}}. \quad (64)$$

In the practically relevant regime where  $T_{j,i}^{\text{edge}} \lesssim D_j$ , the operator  $[\cdot]_+$  is active and

$$G_{j,i}^A = v_j - v_j \frac{t_{j,i}^{\text{tx}}}{D_j} - v_j \frac{t_{j,i}^{\text{comp}}}{D_j}. \quad (65)$$

Using  $t_{j,i}^{\text{comp}} = \theta_{j,i} \tau_i(y_i)$ , we obtain

$$G_{j,i}^A = \underbrace{v_j - v_j \frac{t_{j,i}^{\text{tx}}}{D_j}}_{\text{independent of } y_i} - \underbrace{v_j \frac{\theta_{j,i}}{D_j} \tau_i(y_i)}_{\text{congestion-dependent term}}. \quad (66)$$

Adding the energy-saving term  $c_{j,i}^{\text{A,save}} = E_j^{\text{loc}} - E_{j,i}^{\text{tx}}$  with coefficient  $\nabla_e^A$  and subtracting the payment, the full MaU utility can be written as

$$U_{j,i}^A = \bar{S}_j(\dot{i}) - \kappa_j \theta_{j,i} \tau_i(y_i) - p_{j,i}, \quad (67)$$

where

$$\bar{S}_j(\dot{i}) = v_j - v_j \frac{t_{j,i}^{\text{tx}}}{D_j} + \nabla_e^A c_{j,i}^{\text{A,save}}, \quad \kappa_j = \frac{v_j}{D_j} > 0. \quad (68)$$

Thus, MaUs share the same congestion structure as HuUs, with user-specific  $\kappa_j$ . This linearization preserves the *ordinal* ranking of actions induced by the original soft-deadline utility in the operating regime of interest, and hence does not change the set of Nash equilibrium.

### E. Sign Consistency of Congestion Terms

The ordinal-potential property relies on the fact that congestion terms in the utility and in the potential move in the same direction.

**Lemma 2** (Sign consistency). *For deviation  $\pi_j : \dot{i} \rightarrow \dot{i}'$ , the congestion part of the utility change,*

$$-\kappa_j \theta_{j,i'} \tau_i(y_{i'}(\pi')) + \kappa_j \theta_{j,i} \tau_i(y_i(\pi)),$$

*and the congestion-integral term in the potential change,*

$$-\left( \int_{y_{i'}(\pi)}^{y_{i'}(\pi) + \gamma_{j,i'}} \tau_i(z) dz - \int_{y_i(\pi) - \gamma_{j,i}}^{y_i(\pi)} \tau_i(z) dz \right),$$

*have the same sign.*

*Proof.* Apply Lemma 1 to both integrals. Each integral lies between a lower and an upper pointwise congestion term. After scaling by the positive factors  $\kappa_j \theta_{j,i} / \gamma_{j,i}$  and  $\kappa_j \theta_{j,i'} / \gamma_{j,i'}$ , the corresponding bounds match the pointwise expressions in the lemma. Hence the two congestion components must share the same sign. ■

For the linear model  $\tau_i(y) = y/f_i^{\text{On}}$ , the result is even more transparent: the integral is simply the area under a straight line, so shifting traffic to a more congested SP increases both the user's delay and the integrated congestion cost.

### F. Monotonicity and Convexity of SP Cost

The SP-cost term  $K_i(\cdot)$  is chosen to discourage load concentration on heavily utilized SPs.

Assume  $K_i : \mathbb{R}_+ \rightarrow \mathbb{R}_+$  is increasing and convex. Then for  $x'_i = x_i - r_j$  and  $x'_{i'} = x_{i'} + r_j$ ,

$$K_{i'}(x_{i'} + r_j) - K_{i'}(x_{i'}) \geq 0, \quad K_i(x_i) - K_i(x_i - r_j) \geq 0. \quad (69)$$

Convexity further implies that the marginal cost  $K_i(x + \Delta) - K_i(x)$  is nondecreasing in  $x$ : adding the same workload to a more congested SP incurs a larger cost. Consequently,

$$-\left[ K_{i'}(x_{i'} + r_j) - K_{i'}(x_{i'}) \right] + \left[ K_i(x_i) - K_i(x_i - r_j) \right] \quad (70)$$

moves in a direction consistent with the deviation: shifting load towards a more congested SP is penalized in the potential.

For the linear model  $K_i(x) = \omega_1 e_i^{\text{comp}} x / f_i^{\text{On}}$ , these increments are simply proportional to  $r_j$  and preserve the sign.

### G. Proof Sketch of Theorem 1

We are now ready to justify the ordinal-potential property.

Consider a deviation  $\pi_j : i \rightarrow i'$  that strictly increases SD  $u_j^{\text{On}}$ 's utility, i.e.,  $\Delta U_j > 0$  in (62). Comparing (62) and (63), we note:

- The non-congestion term  $S_j(i') - S_j(i)$  appears identically in both  $\Delta U_j$  and  $\Delta \Phi$ .
- By Lemma 2, the congestion contributions to  $\Delta U_j$  and  $\Delta \Phi$  have the same sign.
- By Appx. D-F, the SP-cost variation responds monotonically and convexly to the direction of load shift, further aligning the sign of  $\Delta \Phi$  with that of  $\Delta U_j$ .
- Payment differences  $-(p_{j,i'} - p_{j,i})$  only redistribute welfare and are excluded from  $\Delta \Phi$  (Appx. D-I), so they do not affect the ordinal comparison.

Hence,  $\Delta U_j > 0$  implies  $\Delta \Phi > 0$ , which proves that  $\Phi(\pi)$  is an *ordinal potential* for the considered game, as stated in Theorem 1.

### H. Finite-Improvement Property and Existence of NE

The ordinal-potential property directly yields convergence of better-response dynamics and existence of pure-strategy Nash equilibria.

Let  $\mathcal{A}_j = \{0\} \cup \mathcal{S}^{\text{On}}$  be SD  $u_j^{\text{On}}$ 's finite action set, and  $\mathcal{A} = \prod_j \mathcal{A}_j$  the joint action space. Consider any strict better-response dynamics in which, at each step, some SD switches to an action that strictly improves its utility. By Theorem 1, every such deviation strictly increases the potential  $\Phi(\pi)$ .

Since  $\mathcal{A}$  is finite, the sequence of potential values cannot increase indefinitely. The process must terminate after finitely many steps at a profile  $\pi^*$  where no SD can further increase its utility via a unilateral deviation. By definition,  $\pi^*$  is a pure-strategy NE. Moreover, any local maximizer of  $\Phi(\pi)$  is a pure-strategy NE, because any unilateral move would reduce (or not increase)  $\Phi$ , and hence would not increase the deviator's utility in an ordinal-potential game.

This finite-improvement property underpins PG-BRD: as long as SDs occasionally update their actions based on (approximate) best responses, the algorithm converges in finitely many steps to a stable congestion-aware offloading configuration.

### I. Treatment of Monetary Payments in the Potential Function

We finally clarify why monetary payments are left out of the potential, which is sometimes questioned from a mechanism-design perspective.

Let  $\mathcal{W}(\pi)$  denote the *non-transfer* welfare:

$$\mathcal{W}(\pi) = \sum_{j: \pi_j \neq 0} S_j(\pi_j) - \sum_i \int_0^{y_i(\pi)} \tau_i(z) dz - \sum_i K_i(x_i(\pi)). \quad (71)$$

Agent-to-agent payments  $\{p_{j,i}\}$  are internal transfers between SDs and SPs. In the absence of external taxes or subsidies, they sum to zero at the system level and do not affect  $\mathcal{W}(\pi)$ . Thus,

payments can be omitted from the potential without changing ordinal comparisons between profiles.

In other words,  $\Phi(\pi)$  is designed as a proxy for *real* system efficiency, capturing latency savings, energy savings, congestion, and SP costs, while treating payments as a separate distributional layer superimposed on top of this efficiency metric. This follows standard practice in congestion and resource-allocation games and allows PG-BRD to focus on aligning individual incentives with global performance, independently of how the resulting welfare is split among participants.